Int J Appl Earth Obs Geoinformation 87 (2020) 102053

Contents lists available at ScienceDirect

Int J Appl Earth Obs Geoinformation

journal homepage: www.elsevier.com/locate/jag

How much variation in land surface phenology can climate oscillation modes explain at the scale of mountain pastures in Kyrgyzstan?

Monika A. Tomaszewska[a], Geoffrey M. Henebry[b,c,*]

[a] Geospatial Sciences Center of Excellence, South Dakota State University, Brookings, SD, 57007, USA
[b] Department of Geography, Environment, and Spatial Sciences, Michigan State University, East Lansing, MI, 48824, USA
[c] Center for Global Change and Earth Observations, Michigan State University, East Lansing, MI 48823, USA

ARTICLE INFO

Keywords:
Land-atmosphere interactions
Snow seasonality
Terrain effects
Montane Central Asia
Landsat
MODIS
Modeling

ABSTRACT

Climate oscillation modes can shape weather across the globe due to atmospheric teleconnections. We built on the findings of a recent study to assess whether the impacts of teleconnections are detectable and significant in the early season dynamics of highland pastures across five rayons in Kyrgyzstan. Specifically, since land surface phenology (LSP) has already shown to be influenced by snow cover seasonality and terrain, we investigated here how much more explanatory and predictive power information about climatic oscillation modes might add to explain variation in LSP. We focused on seasonal values of five climate oscillation indices that influence vegetation dynamics in Central Asia. We characterized the phenology in highland pastures with metrics derived from LSP modeling using Landsat NDVI time series together with MODIS land surface temperature (LST) data: Peak Height (PH), the maximum modeled NDVI and Thermal Time to Peak (TTP), the quantity of accumulated growing degree-days based on LST required to reach PH. Next, we calculated two metrics of snow cover seasonality from MODIS snow cover composites: last date of snow (LDoS), and the number of snow covered dates (SCD). For terrain features, we derived elevation, slope, and TRASP index as linearization of aspect. First, we used Spearman's rank correlation to assess the geographical differentiation of land surface phenology metrics responses to environmental variables. PH showed weak correlations with TTP (positive in western but negative in eastern rayons), and moderate relationships with LDoS and SCD only in one northeastern rayon. Slope was weakly related to PH, while TRASP showed a consistent moderate negative correlation with PH. A significant but weak negative correlation was found between PH and SCAND JJA, and a significant weak positive correlation with MEI MAM. TTP showed consistently strong negative relationships with LDoS, SCD, and elevation. Very weak positive correlations with TTP were found for EAWR DJF, AMO DJF, and MEI DJF in western rayons only. Second, we used Partial Least Squares regression to investigate the role of oscillation modes altogether. PLS modelling of TTP showed that thermal time accumulation could be explained mostly by elevation and snow cover metrics, leading to reduced models explaining 55 to 70% of observed variation in TTP. Variable selection indicated that NAO JJA, AMO JJA and SCAND MAM had significant relationships with TTP, but their input of predictive power was neglible. PLS models were able to explain up to 29% of variability in PH. SCAND JJA and MEI MAM were shown to be significant predictors, but adding them into models did not influence modeling performance. We concluded the impacts of climate oscillation anomalies were not detectable or significant in mountain pastures using LSP metrics at fine spatial resolution. Rather, at a 30 m resolution, the indirect effects of seasonal climatic oscillations are overridden by terrain influences (mostly elevation) and snow cover timing. Whether climate oscillation mode indices can provide some new and useful information about growing season conditions remains a provocative question, particularly in light of the multiple environmental challenges facing the agropastoralism livelihood in montane Central Asia.

1. Introduction

Kyrgyzstan (aka the Kyrgyz Republic) spans multiple climatic regimes, from arid/semi-arid deserts to hot, humid continental climates (Peel et al., 2007). Strong spatial variation in precipitation and temperature exists due to orography (Böhner, 2006; Bothe et al., 2012), as the mountain ranges of Tien Shan, Pamir, and Alatau cover more than 90% of the country's land area (Azykova, 2002). Moreover, Central Asia

* Corresponding author at: Department of Geography, Environment, and Spatial Sciences, Michigan State University, East Lansing, MI, 48824, USA.
E-mail address: henebryg@msu.edu (G.M. Henebry).

https://doi.org/10.1016/j.jag.2020.102053
Received 17 October 2019; Received in revised form 26 November 2019; Accepted 6 January 2020
Available online 16 January 2020
0303-2434/ © 2020 The Authors. Published by Elsevier B.V. This is an open access article under the CC BY-NC-ND license (http://creativecommons.org/licenses/BY-NC-ND/4.0/).

(Kazakhstan, Kyrgyzstan, Tajikistan, Turkmenistan, and Uzbekistan) has been identified as a "climate change hot-spot", a region where climate is especially responsive to global change (Bothe et al., 2012; Giorgi, 2006). This "hot-spot" might arise from regional and local feedbacks (e.g., snow-ice albedo feedback and/or soil moisture-precipitation feedback) or to changes in intrinsic variability of atmospheric circulation patterns and oscillation modes (Giorgi, 2006). Interaction of atmosphere and oceans plays an essential role in shaping climate and its variability, including naturally-occurring dynamical modes (Wang and Xie, 2004; Wang and Schimel, 2003), which may also be changing as a result of global warming (Yeh et al., 2018). Large-scale climatic variability is often dominated by a few modes resulting in teleconnections—correlated weather patterns between remote locations (Horel and Wallace, 1981). Teleconnections can play significant roles in determining seasonal weather anomalies, whether warm and dry or wet and cold (Casanueva et al., 2014). The most well-known mode of interannual climatic variability is ENSO (El Niño-Southern Oscillation; (Wang and Xie, 2004), which is generated through coupled interactions between the ocean and atmosphere in the tropical Pacific and alternates between anomalously warm (El Niño) and cold (La Niña) sea surface temperature (SST) conditions (Bjerksen, 1969). Over the Northern Hemisphere during wintertime, the most influential mode is the North Atlantic Oscillation (NAO) (Hurrell, 1995; Hurrell et al., 2003; Rodwell et al., 1999).

Over Central Asia, there are many studies describing the linkages between weather patterns anomalies and climatic oscillations (Barlow et al., 2002; Bothe et al., 2012; Gerlitz et al., 2018). For example, Syed et al. (2006) showed that a positive precipitation anomaly over southwestern Central Asia had been triggered by warm ENSO phase and positive phase of North Atlantic Oscillation. Yin et al. (2014) highlighted the effects of the polar–Eurasian (POL/EUR), and East Atlantic–Western Russia (EAWR) patterns on Central Asian winter climate, which enhanced moisture fluxes. In addition, the EA mode has been shown to be strongly related to ENSO, which makes the investigation of its nature and the independence of its influence more complex (Gerlitz et al., 2018; Iglesias et al., 2014). Li et al. (2008) indicated that the warm phase of the Atlantic Multidecadal Oscillation (AMO) could significantly affect the Indian monsoon rainfall, which could, in turn, affect southern Central Asia (de Beurs et al., 2018).

The agropastoralism, which is the basis of the economy in montane Central Asia, depends critically on precipitation. Herders of the highlands have been practising vertical transhumance—the annual cycle of livestock movement to higher elevation pastures (Schillhorn Van Veen, 1995)—to take advantage of seasonally available forage resources. Dependency on pasture resource availability during the short montane growing season makes pastoral livelihoods especially vulnerable to variation and change in environmental conditions and weather patterns. In this semi-arid region where most of the precipitation falls outside of the growing season, changes in precipitation patterns may shift forage availability and shorten growing season (Hoppe et al., 2016; Vetter, 2005; Zhumanova et al., 2018, 2016).

Assessment of changes in local to regional environmental conditions in the highlands of Kyrgyzstan are impeded due to the remoteness of much of the area, a paucity of ground-level data, and the siting of most weather stations in inhabited valleys far from the pasture zones of interest. One solution is to use satellite remote sensing as a source of information. Pasture phenology has often been tracked through modelling of land surface phenology (LSP), which describes the temporal pattern of the vegetated land surface as observed using remote sensing (de Beurs and Henebry, 2010, 2004; Henebry and de Beurs, 2013). A commonly used indicator of green vegetation, the Normalized Difference Vegetation Index (NDVI) is the difference between near-infrared and red reflectance divided (or normalized) by the sum of the reflectances: [NIR − Red]/[NIR + Red] (Buermann et al., 2003; Myneni et al., 1995; Tucker, 1979).

Variability in the timing of LSP and the seasonal amplitude of the NDVI has been linked to changes in weather and climate within Central Asia (Bohovic et al., 2016; de Beurs et al., 2018,de Beurs et al., 2015 de Beurs and Henebry, 2008; Jiang et al., 2017; Kariyeva et al., 2012; Kariyeva and van Leeuwen, 2011; Lu et al., 2014). Studies have shown that fluctuations in LSP can be related to large scale climate oscillations at various extents over Central Asia and other regions (Buermann et al., 2003; Cook et al., 2005; de Beurs et al., 2009; Gong and Shi, 2003; Li et al., 2016; Menzel et al., 2005; Viña and Henebry, 2005; Wright et al., 2014). de Beurs and Henebry (2008) showed the Arctic Oscillation (AO) appears to affect the NDVI peak (modelled seasonal maximum of the NDVI index) over the Asian part of northern Eurasia more strongly than the NAO. Wright et al. (2014) found that early season vegetation productivity measured using NDVI over the Eurasian wheat belt is linked to both the winter (December–February) and early summer (April–June) phases of the NAO. Their results have shown that land surface anomalies preceding the Russian heatwave in 2010 were consistent with highly negative anomalies of NAO. More recently, de Beurs et al. (2018) analyzed the importance of five climate modes (NAO, EAWR, AMO, Scandinavian [SCAND], and ENSO), both together and separately, on precipitation, temperature, and land surface phenology to discover where each climate index had more influence across the Central Asian region. They used a downward-arching convex quadratic (CxQ) function to model the observed land surface phenology and to derive, as a phenological metric, the Peak Height (PH) – the maximum modelled NDVI. Then, they linked this phenometric with seasonal (winter, spring, and summer) values of five oscillation indices. As a result, they reported a percentage of land area in Central Asia that exhibited a significant correlation between each seasonal mode index and PH over at least 10% of the study area. Their maps that show multivariate climate oscillation impacts on land surface phenology and weather (seasonal temperature and precipitation). Across Kyrgyzstan, they reported a significant R^2 around 0.4.

While de Beurs et al. (2018) found indications of significant teleconnected influence on precipitation in montane Central Asia, the scale of analysis was spatially coarse. The precipitation and temperature data they used were gridded to 0.5° and the NDVI data were nominally 100 times finer (0.05°) in area. Here, we aim to test whether the linkages identified in de Beurs et al. (2018) as important for explaining observed temperature and precipitation anomalies at the regional scale translated to the scale of mountain pastures using finer resolution remote sensing data and, thus, might be able to inform decision-making by herders and pasture committees. Specifically, our question is whether the impacts of oscillation anomalies are detectable and significant in the mountain pastures using LSP metrics based on much finer spatial resolution data. We have already shown that land surface phenology is influenced by snow cover seasonality and terrain (Tomaszewska et al., 2019). Thus, we investigate here how much more explanatory power some information about oscillation modes might add to explain LSP in mountain pastures of Kyrgyzstan. The time frame of this study extends from 2000/01 to 2017.

2. Materials and methods

2.1. Study area

The area of the study focuses on pasturelands spanning over five districts (called rayons): Chong-Alay (4,850 km^2), Alay (7,554 km^2), Kara-Kulja (5,739 km^2), At-Bashy (19,030 km^2), and Naryn (7,872 km^2) in the highlands of Kyrgyzstan in montane Central Asia. We selected these rayons because they represent a range of climatic conditions due to geographic location and elevation (cf. Fig. 1). According to the Köppen-Geiger climate classification system (Peel et al., 2007): Chong-Alay and Alay are under the cold desert climate (BWk), while the eastern part of Alay is also impacted by cold semi-arid climate (BSk) and warm continental/humid continental climate (Dfa). Most of Kara-Kulja lies under warm continental climate (Dsa). The large extent of At-

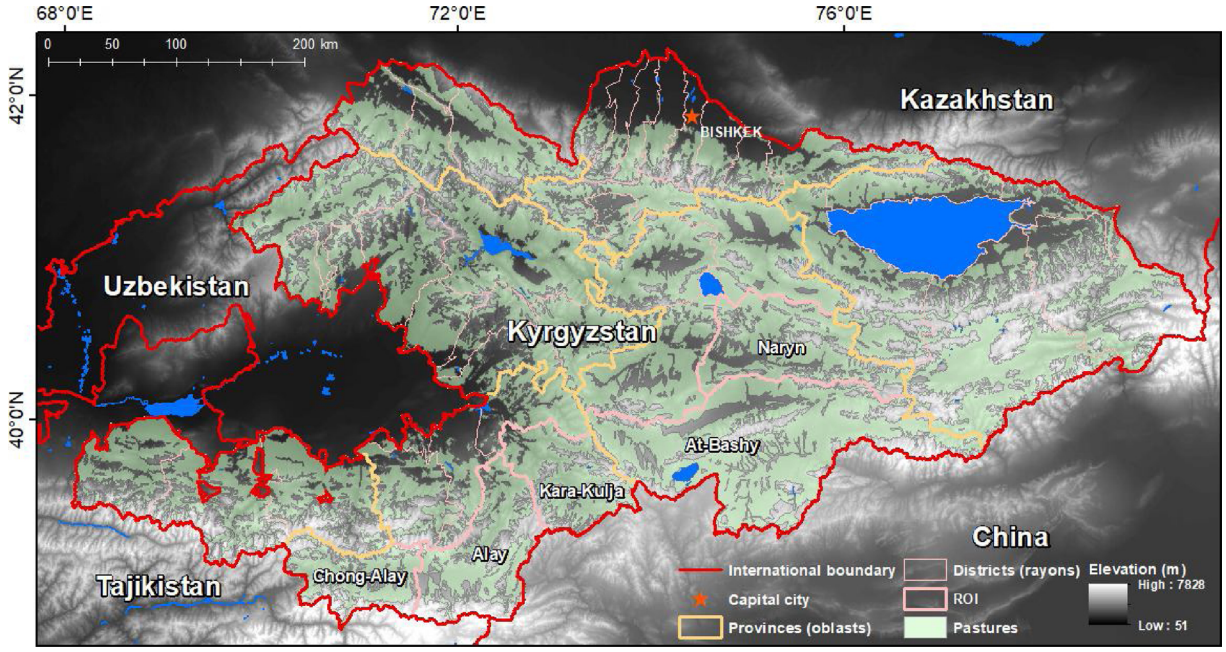

Fig. 1. The study area is the pasture land use area in Kyrgyzstan; it is displayed in light green (from Asian Development Bank, 2010a, 2010b) and draped over the SRTM 30 m DEM (Projected coordinate system: Albers Conic Equal Area). Selected rayons of interest (ROI) are labelled and marked in light pink.

Bashy includes temperate continental climate/Mediterranean continental climate (Dsb), temperate continental/humid continental climate (Dfb), cold semi-arid climate (BSk) and, at the very southern part, cold desert climate (BWk). Naryn is a mixture of temperate continental/humid continental climate (Dfb) and cold semi-arid climate (BSk).

In addition, we visited four of these rayons during two field campaigns: Naryn and At-Bashy in July 2016, and Chong-Alay and Alay in July 2017. Information about the extent of pasture land use was acquired from Soviet-era land use map that had been updated in 2008 within the CACILM project (Asian Development Bank, 2010a, 2010b) using remote sensing data from Landsat 7 ETM + and MODIS.

2.2. Data

We used multiple geospatial datasets and climate oscillation mode information.

2.2.1. Geospatial data

Metrics of land surface phenology, snow seasonality, and terrain information were supplied by the previous work (Tomaszewska et al., 2019; Tomaszewska and Henebry, 2018).

Metrics of snow seasonality were generated using 500 m MODIS (MOD10A2) Terra snow cover 8-day composites (Riggs and Hall, 2015) distributed by the National Snow and Ice Data Center (https://nsidc.org/). Using the Normalized Difference Snow Index (NDSI) (Hall et al., 2002; Riggs and Hall, 2004), the MOD10A2 product reports the maximum snow cover extent observed during 8-day period by compositing observations from the MODIS/Terra Snow Cover Daily L3 Global 500 m Grid product (MOD10A1 V006). We downloaded two MODIS tiles (h23v04 and h23v05) from the middle of 2000 to the end of 2017, where each annual dataset consisted of 46 8-day composites. After tile merging, we projected them into the Albers Conic Equal Area coordinate system to 30 m pixel resolution using nearest neighbor resampling. We then extracted in each composite all pixels flagged as "snow" (i.e., pixel value = "200").

To generate the metrics of land surface phenology, we used two groups of products: (1) MODIS Land Surface Temperature, and (2) Landsat Surface Reflectance.

MODIS/Terra and MODIS/Aqua Land Surface Temperature/Emissivity (MOD11A2/MYD11A2 V006) products at 1 km spatial resolution provided an average 8-day land surface temperature (LST) from all MOD11A1/MYD11A1 LST pixels collected within the 8-day period (Wan et al., 2015). We downloaded two MODIS tiles (h23v04 and h23v05) from 2001 for MODIS/Terra and from 2002 for MODIS/Aqua through the end of 2017. After merging, we removed poor quality pixels using the quality bits provided in each product, converted land surface temperature from Kelvin to °C, and projected the data into the Albers Conic Equal Area coordinate system with 30 m pixel resolution using bilinear resampling.

We used the Landsat Collection 1 Tier 1 Level-1 Precision and Terrain (L1TP) corrected product from 2001 to the end of 2017. The Collection contains Level-1 data products generated from Landsat 5 Thematic Mapper (TM), Landsat 7 Enhanced Thematic Mapper Plus (ETM+), and Landsat 8 Operational Land Imager (OLI) (USGS EROS, 2017). Surface reflectance NDVI data were obtained by downloading 13,285 images in 33 unique tiles (WRS-2 Paths 147–155 and Rows 30–33) from the USGS Earth Resources Observation and Science (EROS) Center Science Processing Architecture (ESPA) On Demand Interface (https://espa.cr.usgs.gov/). After masking out poor quality pixels using quality bits delivered with each product, we projected the data into the Albers Conic Equal Area coordinate system. Further, to adjust Landsat 5 TM surface NDVI and Landsat 7 ETM+ surface NDVI to the surface Landsat 8 OLI NDVI, which showed to have higher surface reflectance values, we applied the inter-calibration equation from Roy et al. (2016) to both surface NDVI from Landsat 5 TM and Landsat 7 ETM+ scenes. The same equation was used with both datasets because differences between those data were very small (Fisher et al., 2006; Melaas et al., 2013).

For the terrain representation, we downloaded 133 tiles of SRTMGL1, the NASA Shuttle Radar Topography Mission Global 1 arc second (~30 m) V003 product (NASA, 2013) from USGS Earth Explorer (https://earthexplorer.usgs.gov/). Tiles were merged and projected into the Albers Conic Equal Area coordinate system using bilinear resampling to 30 m spatial resolution. Further, we generated two layers of terrain features: slope and aspect (both in degrees). Because aspect is a circular measure, we used a linear transformation to get a continuous measure from 0 to 1, where '0' is assigned to the aspect facing a north-northeast direction—typically, the coolest and wettest orientation in

this landscape—and a value of '1' for the hotter, drier south-south-westerly slopes (1). That measure, called Topographic Solar Radiation Aspect Index (TRASP) (Roberts and Cooper, 1989), is calculated:

$$TRASP = [1 - \cos((\pi/180) \times (a - 30))]/2 \quad (1)$$

where a is aspect in degrees. If there was no aspect (flat area = '-1'), then the value of TRASP was set to 0.5. In addition, we reclassified elevation into six classes (<1800 m, 1800–2400 m, 2400–2900 m, 2900–3400 m, 3400–4000 m, and >4000 m).

2.2.2. Oscillation data

Following de Beurs et al. (2018), we examined standardized anomaly time series of five climate oscillation indices to capture two regional (SCAND, EAWR) and three global (NAO, AMO, MEI) patterns that were found important in Central Asia.

SCAND The Scandinavia (SCAND) regional pattern, also known as Eurasia-1 (Barnston and Livezey, 1987), consists of a primary circulation center over Scandinavia with weaker centers of the opposite sign over western Europe and eastern Russia/western Mongolia. The positive phase of SCAND is associated with positive 500-hPa geopotential height anomalies sometimes reflecting anticyclones (a weather system with high atmospheric pressure in the center) over Scandinavia and western Russia. Geopotential heights approximate the actual height of a pressure surface above mean sea-level. Colder air masses have lower heights; warmer air masses have higher heights. Positive phase of SCAND is linked to below-average temperatures across central Russia and western Europe, and also associated with above-average precipitation across central and southern Europe, but below-average precipitation across Scandinavia (Barnston and Livezey, 1987; CPC-NOAA, 2019; Liu et al., 2014).

EAWR The East Atlantic/West Russia (EAWR) pattern aka Eurasia-2 (Barnston and Livezey, 1987) consists of four main anomaly centers. The positive phase is associated with positive 500-hPa geopotential height anomalies located over Europe and northern China, and negative 500-hPa geopotential height anomalies located over central North Atlantic and north of the Caspian Sea (40°-50° N, 50°-60° E). The positive phase of EAWR exhibits above-average temperatures over eastern Asia and below-average temperatures over large portions of western Russia and northeastern Africa, as well as above-average precipitation in eastern China and below-average precipitation across central Europe (Barnston and Livezey, 1987; CPC-NOAA, 2019; Liu et al., 2014).

NAO The North Atlantic Oscillation (NAO) consists of a north-south dipole of anomalies, with one center located over Greenland and the other center of opposite sign spanning the central latitudes of the North Atlantic between 35° N and 40° N (centered on the Azores). The positive phase of the NAO indicates below-average 500-hPa geopotential height and surface pressure across the high latitudes of the North Atlantic and above-average heights and pressure over the central North Atlantic, eastern United States, and western Europe. Together they generate a larger-than-average meridional pressure gradient, causing stronger-than-average midlatitude surface westerlies across the Atlantic onto Europe (Wang and Xie, 2004). Strong positive phases of the NAO tend to produce above-average temperatures in the eastern United States and across northern Europe, and below-average temperatures in Greenland as well as across southern Europe and the Middle East. They are also associated with above-average precipitation over northern Europe and Scandinavia during the winter, and below-average precipitation over southern and central Europe (Hurrell et al., 2003; National Weather Service, 2019; Wang and Xie, 2004).

AMO The Atlantic Multi-Decadal Oscillation (AMO) is a series of long-duration changes in the sea surface temperature of the North Atlantic, composed of alternating cool and warm phases that may last for 20–40 years at a time. In general, during positive AMO phases, sea surface temperature (SST) is anomalously warm over most of the North Atlantic ocean, low pressure extends over the Atlantic between 20° S-50° N, wind speeds are reduced over the tropical Atlantic, and precipitation is enhanced in the eastern tropical Atlantic (Alexander et al., 2014; Kerr, 2000).

MEI Multivariate ENSO Index (MEI) describes the status of the El Niño/Southern Oscillation. It combines five oceanic and atmospheric variables: sea level pressure (SLP), sea surface temperature (SST), zonal and meridional components of surface winds, and outgoing longwave radiation (OLR) over the tropical Pacific basin (30° S-30° N, 100° E-70° W). Anomalously positive MEI events (El Niño) include (1) anomalously warm SSTs across the east-central equatorial Pacific, (2) anomalously high SLP over Indonesia and the western tropical Pacific and low SLP over the eastern tropical Pacific, (3) reduction or even reversal of tropical Pacific easterly winds (trade winds), (4) suppressed tropical convection (positive OLR anomalies) over Indonesia and Western Pacific and enhanced convection (negative OLR anomalies) over the central Pacific (ERL-NOAA, 2019; Kobayashi et al., 2015; Wolter and Timlin, 2011, 1993). During anomalously negative phases (La Niña), roughly opposite conditions occur.

From the National Oceanographic and Atmospheric Administration (NOAA) Climate Prediction Center (https://www.cpc.ncep.noaa.gov/data/teledoc/teleindcalc.shtml), we obtained monthly values of SCAND, EAWR, and NAO from 2000 through 2017. From the NOAA Earth Research Laboratory, we downloaded for 2000 through 2017, monthly AMO values (https://www.esrl.noaa.gov/psd/data/timeseries/AMO/) and bimonthly MEI values (https://www.esrl.noaa.gov/psd/enso/mei.old/table.html). Each index was then summarized into seasonal average value of standardized anomaly for winter (DJF), spring (MAM), and summer (JJA). In our study, we did not include the autumn season (SON), following de Beurs et al. (2018). Based on Tables 3 and 4 in de Beurs et al. (2018), we selected those nine of 15 seasonal indices (five oscillation indices × three seasons) that exhibited significant (p-value< 0.1) Spearman correlations with the Peak Height phenometric or seasonal (spring or summer) precipitation or temperature across at least 10% of Central Asia (Table 1). Fig. 2 presents seasonal oscillation annual values of these selected indices.

2.3. Methods

The approaches to generate land surface phenology metrics and snow cover seasonality metrics has been detailed elsewhere (Tomaszewska et al., 2019; Tomaszewska and Henebry, 2018). Here, we provide a general but concise description of those techniques.

2.3.1. Snow cover seasonality metrics

We defined the snow observation period from day of year (DOY) 169—approximately the summer solstice and aligns with MODIS composite dates—and extends to DOY 168 in the following year (i.e.,

Table 1
Oscillation indices shown in de Beurs et al. (2018) to be significant at p-value < 0.1 across at least 10% of Central Asia area, and the direction of their Spearman correlations with the Peak Height phenometric and with spring or summer precipitation or temperature. **Pos is positive**, Neg is negative, *ns is not significant*, and — is not selected.

Index	Season	PH	Precipitation		Temperature	
			MAM	JJA	MAM	JJA
SCAND	DJF	neg	neg	*ns*	*ns*	*ns*
SCAND	MAM	**pos**	**pos**	**pos**	*ns*	neg
SCAND	JJA	neg	—	neg	—	*ns*
EAWR	DJF	**pos**	*ns*	*ns*	*ns*	neg
AMO	DJF	**pos**	**pos**	**pos**	*ns*	*ns*
AMO	JJA	neg	—	*ns*	—	**pos**
NAO	JJA	**pos**	—	neg	—	neg
MEI	DJF	**pos**	**pos**	**pos**	*ns*	*ns*
MEI	MAM	**pos**	**pos**	*ns*	*ns*	*ns*

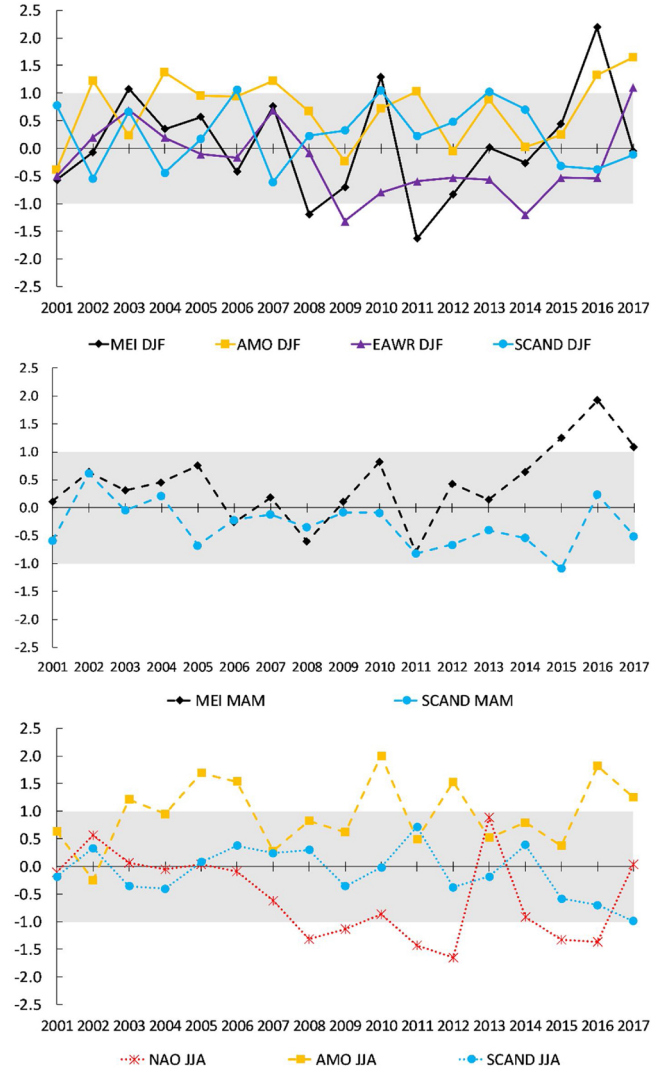

Fig. 2. Annual seasonal values of selected indices. Upper: December to February; middle: March to May; bottom: June to August. Values reflect standardized anomalies of variables used for indices calculation; values between -1 to 1 on grey background. Positive values indicate a positive phase; negative values indicate a negative phase.

$DOY_{169year}$ through $DOY168_{year+1}$). For each snow observation period, we calculated four temporal metrics: the First Date of Snow (FDoS) as the first composite during the snow observation period in which snow cover is detected; the Last Date of Snow (LDoS) as the last composite during the snow observation period in which snow cover is detected; the Duration of Snow Season (DoSS) as the timespan between the FDoS and LDoS; and the Snow-Covered Dates (SCD) as the number of times snow cover was detected within the snow season. Further, we multiplied the number of composites with snow detected by 8 since the compositing period is composed of 8 days, although we realize that this count may be an overestimate. For this study, we have focused only on SCD and LDoS since they have shown stronger relationships with the phenometrics (Tomaszewska et al., 2019).

2.3.2. Land surface phenology

To characterize land surface phenology, we used a downward-arching convex quadratic (CxQ) function (de Beurs and Henebry, 2004; Henebry and de Beurs, 2013) that captures well the seasonal course of insolation at the middle to higher latitudes (de Beurs and Henebry, 2004; Henebry and de Beurs, 2013; Krehbiel et al., 2017; Krehbiel and Henebry, 2016; Nguyen et al., 2018). The model used Landsat surface reflectance data to calculate the NDVI as a proxy for active green vegetation and MODIS LST to calculate accumulated growing degree-days (AGDD) as a proxy for insolation. Land surface temperature during the growing season is highly correlated with insolation in extratropical regions, and grassland plants experience the thermal environment close to the ground (Henebry, 2013; Still et al., 2014). First, we calculated the mean MODIS LST of two daytime and nighttime observations from Terra and Aqua into mean MODIS LST based on (2):

$$\text{mean LST} = [\max(\text{LST@1030}, \text{LST@1330}) + \min(\text{LST@2230}, \text{LST@0130})]/2 \quad (2)$$

We further filtered out mean MODIS LST below 0 °C and calculated the growing degree-days GDD (3) at compositing period t as the maximum of mean LST and T_{base}, which was set to 0 °C (Goodin and Henebry, 1997; Henebry and de Beurs, 2013). Next, we multiplied by 8 each of 46 GDD composites to account for the 8-day compositing period of the MODIS product and accumulated them across the year (4). AGDD was set to zero at the start of each year. These steps generated 17 annual time series of AGDD in °C.

$$GDD_t = \max((\text{mean } LST_t - T_{base}), 0) \quad (3)$$

$$AGDD_t = AGDD_{t-1} + (GDD_t \times 8) \quad (4)$$

Having prepared the AGDD and NDVI, we proceeded to model LSP at each pixel and for each year from 2001 to 2017 as a quadratic function shown in (5):

$$NDVI = \alpha + \beta \times AGDD + \gamma \times AGDD^2 \quad (5)$$

For each pixel in the study area, we used the fitted parameter coefficients—intercept (α), slope (β), and quadratic (γ)—to calculate two LSP metrics (or phenometrics): Peak Height [$PH = \alpha - (\beta^2/4\gamma)$], the maximum modeled NDVI; and Thermal Time to Peak [$TTP = -\beta/2\gamma$], the quantity of AGDD required to reach PH, corresponds to duration of modeled green-up phase. In the model fitting process, we used set of quality criteria and iterative data filtering to obtain optimal model fits (Tomaszewska et al., 2019). We accepted the fitted model only when it passed all six of the following criteria: (i) the quadratic parameter (γ) was less than 0; (ii) the TTP greater than the AGDD of the first observation; (iii) the adjusted R^2 greater than 0.7; (iv) the Root Mean Square Difference (RMSD) less than 0.08; (v) the PH below 1.0; and (vi) at least three observations were distributed before and at least three after the PH.

If any criterion was not fulfilled during the fitting, then the last observation was removed from the dataset, and the model fitting was rerun over the filtered dataset. We then summarized each annual fit by a binary variable (i.e., 0 = no fit, 1 = fit) to generate a final map of the total number of years with successful fits for each pixel. We then arbitrarily divided the modeling results into three groups based on the data distribution: (i) Highly Persistent (HP) pastures with 11–17 years of successful fits out of 17 years of observations, (ii) Persistent (P) pastures with 5–10 years, and (iii) Rarely Available (RA) pastures with just 1–4 years of successful fits. Here, we focused only on Highly Persistent (HP) and Persistent (P) pastures (Fig. 3, Table 2).

Because of the limited or absent area of pastures below 1800 m and above 4000 m in some rayons, we restricted our focus to pixels located in the four elevation classes between 1800 m and 4000 m, which constitutes more than 98% (17,957 km^2) of the pasture area pixels across the five rayons.

2.3.3. Spearman rank correlation analysis

We analyzed the connections between variables using the non-parametric Spearman's correlation coefficients to assess the geographical differentiation of land surface phenology metrics in response to environmental variables. Spearman's rank correlation method assesses whether a monotonic relationship exists, it works for data showing non-normality, and is robust against outliers (Fieller et al.,

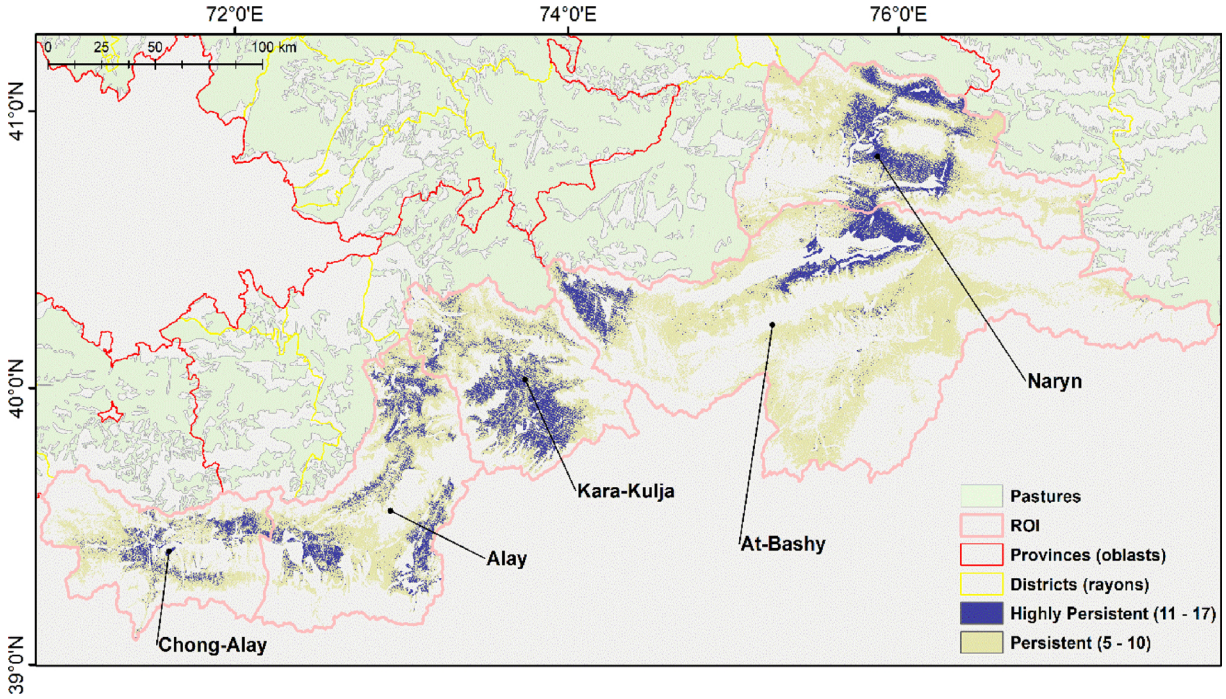

Fig. 3. Study area: all pasturelands in Kyrgyzstan displayed in light green (from Asian Development Bank, 2010a, 2010b), selected rayons of interest (ROI) are labelled, and marked in light pink. In dark purple are pixels from Highly Persistent (HP) pastures, in yellow Persistent (P) pastures. Other pasture classes and land uses within the ROIs not shown.

1957; Lehmann and DöAbrera, 2006).

2.3.4. Partial Least Squares regression modeling

2.3.4.1. Partial Least Squares regression. To analyze how much of variation in land surface phenology metrics can be added to its explanation by the climate oscillation patterns at the scale of mountain pastures, we used the Partial Least Squares (PLS) regression model (Wold, 1966). PLS aims to predict Y variables—in our case, the phenometrics PH and TTP—from X variables (snow cover seasonality metrics, climate oscillation mode standardized anomalies, and terrain variables) and describe their common structure (Geladi and Kowalski, 1986; Wold et al., 2001). It is a technique that generalizes and combines features from principal component analysis (PCA) and multiple linear regression (MLR) (Abdi, 2003). Multiple linear regression aims to minimize sample response prediction error by seeking a linear function of the X variables that explain the variation in response Y; it works well when the X variables are relatively few and mutually uncorrelated. To eliminate the problem of high intercorrelation between variables X (multicollinearity), one of many approaches is a principal component regression, which performs PCA on the X matrix. This statistical procedure uses an orthogonal transformation to find new variables, called principal components, that are linear functions of those in the original dataset, which successively maximize variance and are uncorrelated with each other (Jolliffe and Cadima, 2016; Wold, 1987). Further, PCA approach uses the principal components of X as predictors on response Y. However, this method does not solve the problem of finding an optimal subset of predictors X, because they are chosen to explain X rather than Y. Hence, it does not assure that the principal components that "explain" X are relevant for Y (Abdi, 2003). Therefore, a combination of MLR and PCA seeks to solve that problem.

PLS regression finds components from X that are also relevant for Y. Because correlation has been shown to exist between seasonal oscillations (de Beurs et al., 2018) and between snow metrics—since SCD is determined based on LDoS (Tomaszewska et al., 2019; Tomaszewska and Henebry, 2018), we decided that PLS regression would be a beneficial approach. Specifically, PLS searches for a set of components (also called latent vectors) that performs a simultaneous decomposition of X and Y with the constraint that these components explain as much of the covariance between X and Y as possible (Abdi, 2003). That step generalizes the PCA approach and is followed by a regression step where the decomposition of X is used to predict Y (Abdi, 2003; Wold et al., 2001). However, PLS has no implementation for variable selection, since it aims to find a relevant linear subspace of the predictor variables X, not the variables themselves (Mehmood et al., 2012). In other words, when the dominant source of variation is not related to Y, the maximization of the explained X variance is likely to bring irrelevant information into the PLS model (Tran et al., 2014).

Variable selection methods help to select a small set of highly relevant predictor variables X that are correlated to the response variable Y. Hence, variable selection can improve the estimation accuracy by

Table 2
Combined area of HP and P pastures (km^2) within each rayon.

HP + P Elevation Class	Chong-Alay	Alay	Kara-Kulja	At-Bashy	Naryn	TOTAL
< 1800 m	–	100	241	–	4	345
1800 – 2400 m	45	605	845	381	628	2,504
2400 – 2900 m	522	529	968	898	1,352	4,269
2900 – 3400 m	743	1,166	844	2,743	1,548	7,044
3400 – 4000 m	354	839	212	2,505	230	4,140
> 4000 m	9	4	<1	5	–	18
TOTAL	1,674	3,243	3,108	6,532	3,763	18,320

Table 3
Number of pixels for modelling and testing (split 70:30) over 17 years within each of five studied rayons based on elevation class. In bold, number of pixels used for modeling.

Elevation class	Chong-Alay		Alay		Kara-Kulja		At-Bashy		Naryn	
	Model	*Test*	*Model*	*Test*	*Model*	*Test*	*Model*	*Test*	*Model*	*Test*
1800–2400 m	**2,508**	836	**2,960**	986	**2,734**	911	**2,899**	966	**2,608**	869
2400–2900 m	**2,526**	842	**2,489**	829	**2,962**	987	**3,006**	1,002	**2,848**	949
2900–3400 m	**2,453**	817	**2,647**	882	**2,691**	897	**2,196**	732	**2,524**	841
3400–4000 m	**2,301**	766	**2,457**	819	**2,322**	774	**1,968**	656	**2,064**	688
TOTAL	**9,788**	3,261	**10,553**	3,516	**10,709**	3,569	**10,069**	3,356	**10,044**	3,347

effectively identifying the subset of important predictors and can enhance the model interpretability (Farrés et al., 2015). Here, we based our study on three widely used methods for variable selection to investigate which of the X variables (snow cover seasonality metrics, standardized anomalies of climate oscillation modes, and terrain features) have more significant impact on predicting the phenometrics PH and TTP.

2.3.4.2. Variable selection methods for PLS modeling. The first variable selection method is called "variable influence on projection" or "variable importance in projection" (Wold et al., 1993) usually abbreviated as VIP. The VIP score is a combined measure of how much a variable X contributes to describe the two sets of data: the response variable Y and the predictor variables X. It reflects not only the covariance between X and Y variables but also describes how important that information is for the model of the X variables. The average of the square VIP scores equals to unity, so that value is generally accepted as a threshold value (Andersen and Bro, 2010; Chong and Jun, 2005; Farrés et al., 2015; Mehmood et al., 2012; Rajalahti et al., 2009a; Tran et al., 2014), and we used it here as well.

The second method called the "Selectivity Ratio" (SR) is calculated as the ratio of explained variance to residual variance of X variables on the Y target-projected component. In other words, the method ranks the X variables in relation to their explanation of Y variance. An F-test has been proposed to define the threshold value (Rajalahti et al., 2009b). In order to determine which variable has a high discriminatory ability and to reject the null hypothesis (that explained and residual variances are the same), the calculated F value (F_{calc}), which is equal to SR of variable, has to exceed the critical value for the F distribution, (F_{crit}) = F(1-α, N-2, N-3), where α is the significance level, and N is sample size. The number of degrees of freedom for the numerator (i.e., explained variance) is equal to sample size N minus two degrees of freedom, one because of the calculation of the variable's mean and one because of the introduction of the target-projected component. For the denominator (i.e., residual variance), one additional degree of freedom is lost when the explained variance is subtracted from the original variance of the variable (Farrés et al., 2015; Rajalahti et al., 2009b). Another approach is to set a limit based on explained variance, e.g., for 75% of explained variance, the cut-off value is 3, i.e., 75% of explained to 25% of unexplained variance (Rajalahti et al., 2009a).

The third method of variable selection is to use the classical technique of statistical significance testing that aims to eliminate variables for which the regression coefficient (β) (a single measure of association between each variable X and the response Y) is not significant. To determine significant coefficients, bootstrapping or jackknifing methods (Efron and Tibshirani, 1993; Faber, 2002) are often used (Andersen and Bro, 2010; Mehmood et al., 2012). Based on that method, variables that are not significant at a chosen significance level might be excluded from the model. Additionally, Rajalahti et al. (2009a) propose to use a rule of ±2 standard deviations calculated from the spread of all regression coefficients (if the X variables have the same units). Variables that are within this range can be also excluded.

We employed all three variable selection methods because each of them conveys a bit different information about the variables and the model, and so those methods are expected to yield slightly different results due to the data characteristics (Farrés et al., 2015).

To conduct PLS regression and variable selection, we used the mdatool package v. 0.9.6 in R (Kucheryavski, 2019).

2.3.4.3. Sampling and variables preparation for PLS modeling. First, we merged HP and P pasture masks into one, and cropped it based on the area of each rayon. For each rayon, we randomly selected 400 pixels for each of the four elevation classes (1600 pixels in total) to create a new elevation-based mask. Using each elevational-based mask, we extracted pixels from PH, TTP, LDoS, and SCD for each year (17 in total). Further, we removed pixels with unsuccessful CxQ fits (that yielded no values for PH and TTP), to create a complete dataset. We repeated that procedure four times, once for each elevation class. Then, we divided the datasets into modelling (70%) and testing (30%) subsets (Table 3). Finally, we combined each elevational-based modelling and testing datasets to construct the final datasets, so elevation would serve as a variable X for prediction.

We used 14 metrics as predictor variables X: elevation (m), slope (in degrees), TRASP index (linearized aspect), LDoS, SCD, and the z-scores for each of the following seasonal climate oscillation modes, SCAND DJF, SCAND MAM, SCAND JJA, EAWR DJF, AMO DJF, AMO JJA, NAO JJA, MEI DJF, and MEI MAM.

The PLS regression models were run on standardized data using auto-scaling approach: (1) each variable is scaled to unit variance by dividing them by their standard deviations, and (2) centered by subtracting their averages (Wold et al., 2001), although the final estimated regression coefficients are provided in the original values (Table S1-S2).

Table 4
Spearman correlations between selected pairs of seasonal oscillation modes. The reference correlation is from de Beurs et al. (2018). Rayon specific correlations are extracted from Figs. 4 and 5, and S1-S3. Superscripts after reference correlations: ns = $p > 0.10$; ◊ = $p < 0.10$; * = $p < 0.05$. All rayon specific correlations are significant at $p < 0.05$.

Oscillation Mode Pair	Reference Correlation	Chong-Alay	Alay	Kara-Kulja	At-Bashy	Naryn
SCAND DJF + EAWR DJF	$-0.43^{◊}$	−0.58	−0.58	−0.56	−0.54	−0.53
SCAND DJF + AMO DJF	-0.59^{*}	−0.61	−0.56	−0.55	−0.55	−0.51
SCAND DJF + MEI DJF	-0.20^{ns}	−0.38	−0.32	−0.32	−0.34	−0.29
SCAND DJF + MEI MAM	-0.27^{ns}	−0.40	−0.42	−0.39	−0.38	−0.38
SCAND JJA + MEI MAM	$-0.46^{◊}$	−0.67	−0.69	−0.68	−0.69	−0.70
EAWR DJF + AMO DJF	$+0.36^{ns}$	+0.65	+0.57	+0.57	+0.61	+0.60

We modeled the PH and TTP response variables separately.

Prior to run PLS regression modelling, for each rayon separately, we estimated the association of variables Y and X using Spearman's rank correlation method.

2.3.4.4. PLS regression sequence. The modeling for each phenometric was carried out in four steps: (1) build the initial model using all variables, (2) select fewer but significantly important variables, (3) build three reduced models based on the different variables selected, and (4) compare the results. This procedure was run separately for the two phenometrics in each of five rayons.

It was essential to determine in step one of modeling, the appropriate model complexity to avoid" over-fitting" that would limit generality. The cross-validation (CV) method is a standard procedure to determine a number of significant components (Wold, 1982; Wold et al., 2001, 1984). During CV part, after developing a model, differences between actual and predicted Y-values are calculated for the withheld data. The sum of squares of these differences is computed and collected from all the parallel models to form the predictive residual sum of squares (PRESS), which estimates the predictive ability of the model (Bulut and Alma, 2012; Wold et al., 2001). Then, we applied Wold's R criterion to find the optimal number of significant components based on the specific threshold (0.95) for the ratio of PRESS values between two consecutive components (Abdi, 2003; Bulut and Alma, 2012; Tenenhaus, 1998; Wold et al., 1993).

We used three variable selectors: VIP score with '1′ as the threshold; Selectivity Ratio (SR) with '1.5′ as threshold (ratio of 60% variance explained to 40% of unexplained variance), and 'regression coefficient' method using p-value < 0.05 obtained from jack-knifing and plus or minus one standard deviation—from the mean of all standardized (using auto-scaling) regression coefficients—a slightly less conservative approach compared to Rajalahti et al. (2009a) in the case of cut-offs for the Selectivity Ratio and standard deviation.

3. Results

3.1. Spearman's rank correlation

Figs. 4 and 5, and S1-S3 show a matrix of Spearman's rho coefficients for the X variables (PH and TTP) and the Y variables (two snow cover seasonality metrics, three terrain characteristics, and nine seasonal oscillations) calculated based on the final training (model) dataset for each rayon across elevation classes. Fig. 4 shows the matrix for Chong-Alay, the most southwestern of the five rayons and Fig. 5 shows the correlation matrix for Naryn, the most northeastern rayon (Alay, Kara-Kulja, and At-Bashy appear as Figures S1-S3, respectively).

Peak Height (PH) was effectively decoupled from Thermal Time to Peak (TTP), exhibiting weakly positive correlation in Chong-Alay (Fig. 4), Alay (Figure S1), and At-Bashy (Figure S3), weakly negative in Kara-Kulja (Figure S2), and modestly negative in Naryn (Fig. 5). In Naryn rayon, PH showed a moderate positive relationship with both LDoS and SCD (Fig. 5), but not in any other rayon. PH also exhibited moderate negative relationships with elevation, except in Naryn, where it was moderately positive. Slope was weakly related to PH, except in Alay where it showed a moderate positive relationship (Figure S1). The pattern between PH and TRASP provided a consistent signal across rayons: weak to moderate negative correlation, meaning higher PH on northern and eastern slopes. With respect to the seasonal oscillation indices, there were two patterns consistent across the rayons: weak negative correlation with SCAND JJA and weak positive correlation with MEI MAM. TTP showed consistently strong to very strong negative relationships with LDoS, SCD, and elevation The relationship of TTP with slope was moderately negative except in Alay, where it was weakly positive. TTP showed weak positive correlations with EAWR DJF, AMO DJF, and MEI DJF in the western rayons.

The snow cover seasonality metrics were positively correlated, as expected given that LDoS was used in the determination of SCD. Both snow cover metrics also showed strong positive relationships with elevation and moderate positive relationships with slope (except in Alay, where slope is weakly negative). Relationships with TRASP were weakly negative with SCD (except in At-Bashy were it was not significant) meaning that snow cover stayed longer on northern aspects. For the seasonal climatic oscillation indices, there were weakly negative relationships for both LDoS and SCD with SCAND MAM and AMO DJF (except in At-Bashy and Kara-Kulja) and with SCD only for SCAND JJA in the western rayons of Chong-Alay and Alay.

An interesting feature of each of the correlation matrices was the prevalence of moderately strong to strong positive and negative correlations between the seasonal oscillation mode values. While some of these correlations were not surprising, such as between subsequent seasons of the same oscillation mode index, there were also strong connections—both positive and negative—across different oscillation modes, and their values were not identical across rayons. Note that what is displayed in the correlation matrices constitutes random sample of those pixels that were successful fitted by the CxQ LSP model for some number of years. Thus, each rayon sample was a spatially and temporally random subset of those pixels within the population of pasture land use that were successfully fitted by with the LSP models. In other words, the correlations between seasonal oscillation modes have been "filtered" by a biased spatio-temporal sample within each rayon based on the pixels showing years of good pasture growth.

Table 4 displays the effects of this filtering. The reference correlations are those reported in Table 1 of de Beurs et al. (2018). There was some slight variation in correlation strength across rayons, but all these correlations were significant, even when the reference correlation is not, e.g., SCAND DJF and MEI DJF. Indeed, an effect of the filtering appeared to enhance the signal to noise ratio between the oscillation mode pairs.

3.2. Partial Least Squares regression

Table 5 shows the results of PLS modelling of TTP using R^2 and RMSE based on the testing datasets (30% of the randomly selected pixels and not used for modeling), and the number of components used in the PLS model. In general, the differences between models were small, R^2 ranged from 0.56 to 0.71 across rayons using the initial model. When variable selection methods were applied, it resulted in marginal decreases in R^2 and increases in RMSE. In two instances the variable selection methods yielded the same model: in Alay, SR and RC generated the same model; while in Kara-Kulja, all three variable selection methods resulted in the same outcome. The number of components varied between one and two depending on the rayon. The number of components changed in Alay and At-Bashy after application of variable selection.

Table 6 shows standardized regression coefficients of final models based on three different variable selection methods. Note that values are in decreasing order of coefficient strength. The strongest, elevation was the strongest negative effect on TTP over all methods and rayons, except in Kara-Kulja, where rank order of components is SCD, then LDoS and elevation, all with nearly the same coefficient values. The second coefficient in the other rayons was SCD, generally followed by LDoS. The selectivity ratio method yielded no model with a climatic oscillation index showing any significant impact on TTP. While the RC selection approach indicated moderate to weak positive relationship with NAO JJA in Chong-Alay, At-Bashy, and Naryn. The VIP score pulled in a negligible weak correlation with AMO JJA in Alay and weak negative correlations with SCAND MAM in At-Bashy and Naryn.

For the PLS modeling of PH, Table 7 shows the performance results. In general, R^2 was very low not exceeding 0.2 except in Alay, where the initial model has $R^2 = 0.34$ and $R^2 = 0.29$ for reduced models using either VIP or RC for variable selection. Over the four rayons other than Naryn, the SR method did not indicate any variable to be significant; thus, no model was built. Differences in RMSE between initial and reduced models

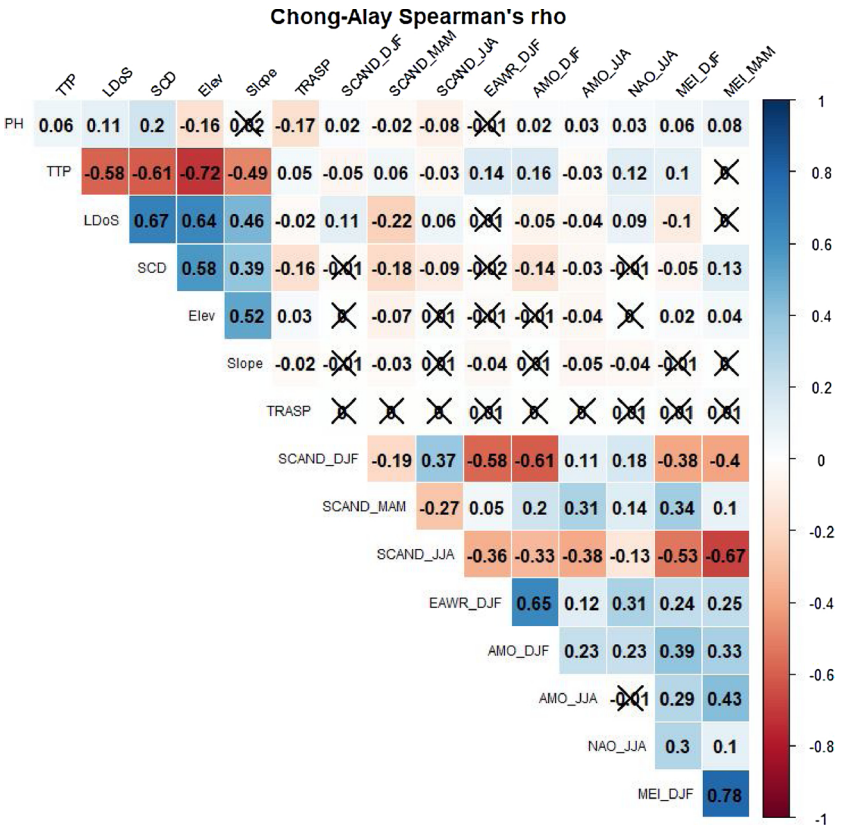

Fig. 4. Spearman's rho coefficient of correlation for Chong–Alay rayon. Significant level at p-value < 0.05 Correlation coefficients with p > 0.05 are crossed out. In reds, negative values of rho; in blues, positive values.

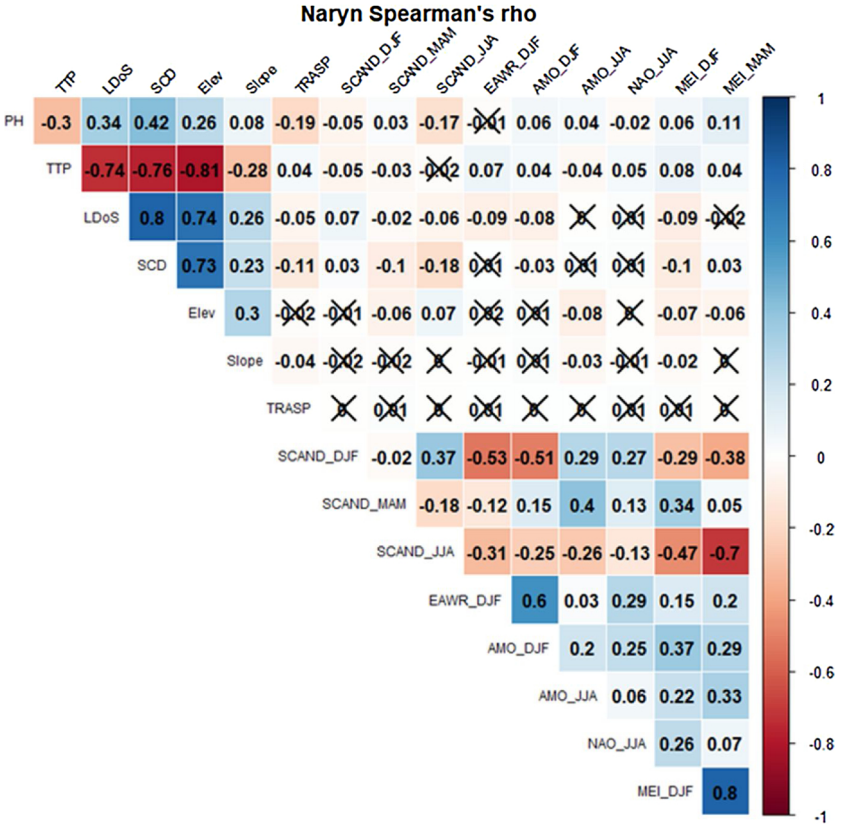

Fig. 5. Spearman's rho coefficient of correlation for Naryn rayon. Significant level at p-value < 0.05 Correlation coefficients with p > 0.05 are crossed out. In reds, negative values of rho; in blues, positive values.

Table 5
Comparison of TTP modelling performance using value of R^2 and Root Mean Square Error (RMSE) based on initial model without variable selection ("Initial"), and three models using different variable selection methods: VIP score ("VIP"), Selectivity Ratio ("SR"), and Regression Coefficients ("RC"). **Same models in bold**.

TTP by Rayon	R^2				RMSE				No. of components			
	Initial	VIP	SR	RC	Initial	VIP	SR	RC	Initial	VIP	SR	RC
Chong-Alay	0.57	0.56	0.55	0.57	252.4	257.1	259	252	2	2	2	2
Alay	0.66	0.64	**0.64**	**0.64**	190.6	197.4	**197.9**	**197.9**	2	1	**1**	**1**
Kara-Kulja	0.56	**0.55**	**0.55**	**0.55**	206.3	**208.6**	**208.6**	**208.6**	1	**1**	**1**	**1**
At-Bashy	0.71	0.70	0.70	0.67	202.6	206.5	205.5	214.7	2	2	2	1
Naryn	0.66	0.66	0.66	0.66	208.8	209.9	210.5	210.7	2	2	2	2

were negligible. Higher R^2 in Alay is related to the higher number of components selected (four components rather than one or two for other rayons) for the initial model. Although in the case of TTP modelling, a higher number of components did not really improve R^2, for PH in Alay and At-Bashy where there were two components used (after variable selection), the R^2 was much higher than in Chong-Alay, Kaka-Kulja and slightly higher in Naryn where only one component was selected.

Table 8 provides the standardized regression coefficients for the PH modelling. Across rayons, the strongest effects are elevation interchanging with SCD, except in Kara-Kulja where TRASP has a negative effect. Elevation negatively affects PH, except in Naryn where its value is positive; whereas, SCD (and LDoS, where selected) shows a positive influence. Slope does not appear in any reduced model. The VIP score method resulted models with negative influence of SCAND JJA in three rayons (Chong-Alay, Kara-Kulja, and At-Bashy) and positive influence of MEI MAM in Chong-Alay and in Kara-Kulja. The SR method selected significant variables only in Naryn: the two snow cover metrics. Note that using only those two variables, the R^2 is comparable to other models for Naryn; moreover, the RMSE is slightly lower than in case of VIP score or RC models.

4. Discussion

In this study, we sought to confirm the findings of de Beurs et al. (2018) regarding linkages between seasonal climate oscillation modes, regional weather, and land surface phenology in Central Asia. Specifically, we focused on the explanatory and predictive power of seasonal climatic oscillations on land surface phenology in highland pastures in Kyrgyzstan from 2001 to 2017. Our question was whether the impacts of oscillation anomalies are detectable and significant in these mountain pastures using LSP metrics based on much finer spatial resolution data. In order to build models that could describe PH and TTP, we included both snow cover seasonality metrics and terrain characteristics, which have already shown to influence on the land surface phenology of highland pastures (Tomaszewska et al., 2019).

The very weak correlations of PH with TTP and PH with snow cover metrics may result in part from calculating the correlations by rayons and across elevation classes. Pasture area in Kyrgyzstan is characterized by complex mountainous terrain that has led to spatially heterogeneous soils and vegetation communities blending into each other (Zhumanova et al., 2018). Thus, at different elevations belts, pasture vegetation types may vary in their NDVI response and their response to snow cover seasonality. For example, the southern part of Alay rayon is an extensive and flat valley bottom traversed by tributaries of the Kyzyl-Suu River, while the northern part is a combination of mountain ridges and intervening valleys along the Gulcha River. Furthermore, given the coarse (1 km) spatial resolution of MODIS LST product relative to the terrain, as a result, any effects of aspect and slope that may be evident at 30 m were blurred across the complex topography at 1 km. The southwestern rayons of Chong-Alay and Alay showed weak positive relationships between TTP and winter values of EAWR and AMO, but these relationships dissipate moving eastward.

Fig. 6 visualizes the mutual relationships among PH, TTP, and SCD by elevation class for Naryn rayon, and Table 9 reports the R^2 values of the simple linear fits illustrated in Fig. 6 for each elevation class alone and considering all classes together. The amount of scatter within each elevation class is substantial, and the effects of elevation on TTP and SCD are clear from Figs. 6B and 6C, respectively. The relatively tight negative relationship between TTP and SCD is not unexpected (Fig. 6C) but note the slope of the relationship across elevation classes is much steeper than the roughly parallel slopes for the four elevation classes. The relationships between PH and SCD are also notable in that the elevation classes between 2400 m and 3400 m exhibit similar steeper slopes; whereas, the other two classes 1800 − 2400 m and 3400 − 4000 m have similar shallower slopes (Fig. 6B). The overall slope splits the difference, but the elevations between 2400 m and 3400 m comprise more than 77% of the pasture land use areas with successful LSP model fits (cf. Table 2). The relationships of PH and TTP show an unexpected positive relationship between 1800 m and 2400 m, but negative relationships at higher elevations. The overall slope is also negative with a slope comparable to 2400 m–2900 m, but shallower than at the higher elevations (Fig. 6A). The negative relationship between TTP and the number of snow cover days can be understood in

Table 6
Standardized (using auto-scaling) regression coefficients for TTP modelling for each rayon based on different variable selection methods. **Same models in bold.** *Positive values in underlined italics.*

VS	Chong-Alay		Alay		Kara-Kulja		At-Bashy		Naryn	
VIP score	Elev	−0.49	Elev	−0.30	**SCD**	**−0.28**	Elev	−0.49	Elev	−0.43
	SCD	−0.23	SCD	−0.30	**LDoS**	**−0.26**	SCD	−0.24	SCD	−0.26
	Slope	−0.09	LDoS	−0.26	**Elev**	**−0.26**	LDoS	−0.21	LDoS	−0.22
	LDoS	−0.06	AMO	−0.01			SCAND	−0.16	SCAND	−0.12
			JJA				MAM		MAM	
Selectivity Ratio	Elev	−0.53	**Elev**	**−0.30**	**SCD**	**−0.28**	Elev	−0.59	Elev	−0.53
	SCD	−0.22	**SCD**	**−0.29**	**LDoS**	**−0.26**	SCD	−0.19	SCD	−0.22
	LDoS	−0.08	**LDoS**	**−0.26**	**Elev**	**−0.26**	LDoS	−0.14	LDoS	−0.15
Regression Coefficient	Elev	−0.42	**Elev**	**−0.30**	**SCD**	**−0.28**	Elev	−0.49	Elev	−0.45
	SCD	−0.24	**SCD**	**−0.29**	**LDoS**	**−0.26**	SCD	−0.41	SCD	−0.25
	NAO	*0.22*	**LDoS**	**−0.26**	**Elev**	**−0.26**	*NAO*	*0.02*	LDoS	−0.19
	JJA						*JJA*		*NAO*	*0.13*
	LDoS	−0.17							*JJA*	

Table 7
Comparison of PH modelling performance using value of R^2 and Root Mean Square Error (RMSE) based on: initial model without variable selection ("Initial"), and three models using different variable selection methods: VIP score ("VIP"), Selectivity Ratio ("SR"), and Regression Coefficients ("RC"), "— "no model built.

PH by Rayon	R^2				RMSE				No. of components			
	Initial	VIP	SR	RC	Initial	VIP	SR	RC	Initial	VIP	SR	RC
Chong-Alay	0.12	0.12	—	0.13	0.157	0.157	—	0.156	1	1	—	1
Alay	0.34	0.29	—	0.29	0.142	0.148	—	0.148	4	2	—	2
Kara-Kulja	0.16	0.12	—	0.14	0.149	0.153	—	0.151	2	1	—	1
At-Bashy	0.18	0.20	—	0.20	0.170	0.167	—	0.168	2	2	—	2
Naryn	0.17	0.16	0.16	0.17	0.149	0.150	0.150	0.149	1	1	2	1

terms of higher albedo associated with snow cover reducing the net radiation at the surface and limiting sensible heat flux. The positive relationship of PH with snow cover days arises from the dependence of the pastures on precipitation that falls outside of the growing season. Most of the annual precipitation falls during the winter and the meltwater from the accumulated snow provides the moisture for the beginning of the growing season. Also, the snowpack insulates the soil surface and retains moisture; thus, having a later snowmelt date, suggesting a larger snowpack, provides more soil moisture enabling greater plant growth (Groffman et al., 2001; Qiao and Wang, 2019).

Given these results, it would be fair to inquire why not model the phenometrics by elevation class. We had three reasons for the approach we took. First, any division of elevation into classes is arbitrary and we wanted to avoid developing "optimized classifications" for each rayon and, thus, increase the possibility of overfitting the data. Second, since terrain complexity is very high in each rayon resulting in variation in phenometrics (sometimes in counterintuitive ways) and so we expected to improve model performance by including a broad range of conditions, especially as TTP follows an elevational gradient. Third, our primary interest was to evaluate the impact of the climate oscillation indices on potentially increasing both explanatory and predictive power.

The PLS modeling of TTP showed that thermal time accumulation was modulated by elevation and snow cover metrics. Those variables alone produced models using SR variable selection that explained 55–70 % of the observed variation in TTP (Table 6). Overall, variable selection brought almost no change in modeling performance; thus, the reduction in variables eliminated those variables that had marginal explanatory and prediction power at the scale of mountainous pastures. VIP score and RC methods showed that specific seasonal oscillation indices could add to model performance, but the differences in R^2 and RMSE were negligible. Recall the VIP score reflects both the covariance between X and Y variables and the importance of each X variable for predicting Y. Therefore, while a variable may add explanatory power of the model itself, it does not necessarily improve the predictive power of the model.

VIP scores indicated that AMO JJA and SCAND MAM had significant negative relationships with TTP in Alay and in the two eastern rayons, respectively. According to de Beurs et al. (2018) AMO JJA showed positive Spearman's correlation with summer temperature. However, the standardized AMO JJA regression coefficient is minimal, and so that impact might be potentially overlooked in the modelling. In our findings SCAND MAM showed a stronger negative relationship with TTP, while in the reference paper, SCAND MAM exhibited a positive relationship with spring and summer precipitation and negative relationship with spring temperature. We may speculate that since high SCAND MAM values were associated with positive precipitation anomalies and negative temperature decreases during spring season (de Beurs et al., 2018), the TTP would decrease during these years with wetter springs.

The RC variable selection methods indicated only NAO JJA to be significant and have a positive regression coefficient with TTP (cf. Table 6); whereas, de Beurs et al. (2018) found a negative relationship with summer temperature (cf. Table 1). It is important to keep in mind that de Beurs et al. (2018) analyzed all five countries of Central Asia, and so our findings for selected rayons in Kyrgyzstan might not have been captured in the broader scale analysis.

In terms of PH, the PLS models after variable selection were able to explain up to 29% of variability in PH. The SR approach, which emphasizes explaining variability in Y, indicated no significant variables X in every rayon other than Naryn where only snow cover metrics were significant. Using VIP score and RC, in the three western rayons, terrain features drove PH; whereas, in the two eastern rayons (At-Bashy and Naryn), the stronger effect appeared from snow cover metrics. It should be mentioned that PH may be influenced by abiotic factors (climate, terrain, recent weather), biotic influences (vegetation community, grazing pressure, unpalatable species), and disturbance history (time since landslide, time since grazing, time since drought) (Henebry, 2019, 2013). Thus, modeling PH is not as straightforward as TTP, which is influenced by temperature and moisture lapse rates.

Again, only two seasonal oscillations were selected as significant: SCAND JJA and MEI MAM. SCAND JJA, according to de Beurs et al. (2018), showed negative correlation with summer precipitation,

Table 8
Standardized (using auto-scaling) regression coefficients for PH modelling for each rayon based on different variable selection methods. *Positive values in underlined italics*.

VS	Chong-Alay		Alay		Kara-Kulja		At-Bashy		Naryn	
VIP score	Elev	−0.18	Elev	−0.86	TRASP	−0.20	*SCD*	*0.46*	*SCD*	*0.17*
	SCD	*0.17*	*LDoS*	*0.47*	Elev	−0.14	Elev	−0.46	*LDoS*	*0.14*
	TRASP	−0.16	*SCD*	*0.19*	SCAND JJA	−0.12	TRASP	−0.19	*Elev*	*0.11*
	SCAND JJA	−0.10			*MEI MAM*	*0.12*	SCAND JJA	−0.07	TRASP	−0.08
	MEI MAM	*0.10*								
Selectivity Ratio	–		–		–		–		*SCD*	*0.39*
									LDoS	*0.01*
Regression Coefficient	Elev	−0.20	Elev	−0.82	TRASP	−0.26	*SCD*	*0.47*	*SCD*	0.17
	SCD	*0.21*	*SCD*	0.60	Elev	−0.19	Elev	−0.46	*LDoS*	0.14
	TRASP	−0.20			*MEI MAM*	*0.16*	TRASP	−0.21	*Elev*	0.11
	SCAND JJA	−0.12			*SCD*	*0.04*			TRASP	−0.08
									SCAND JJA	−0.07

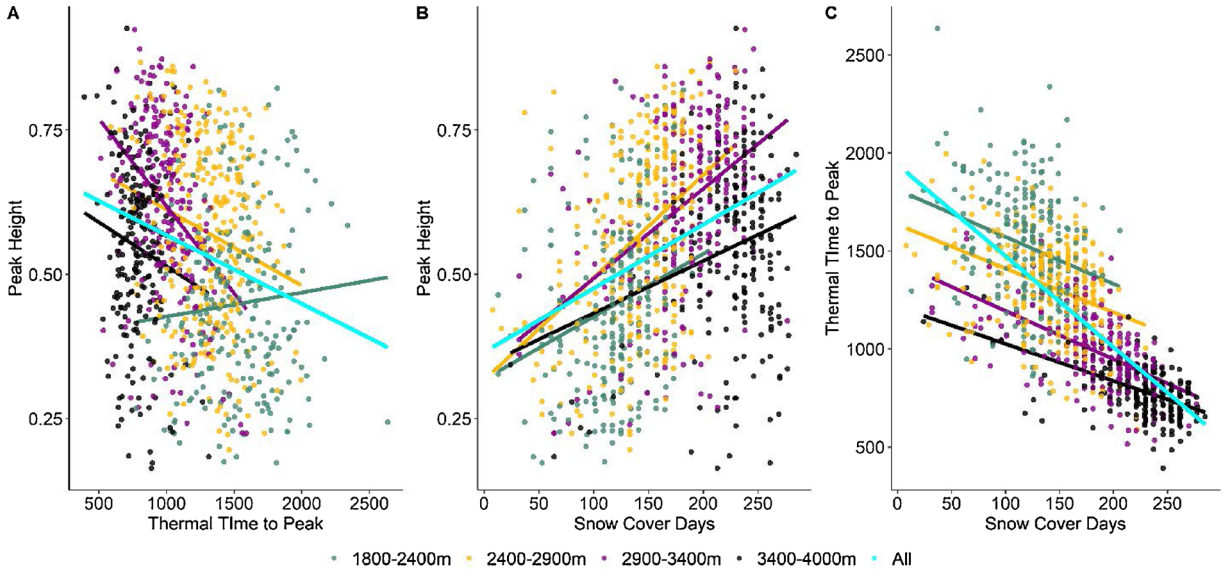

Fig. 6. Randomly sampled 1000 pixels from modeling dataset over Naryn rayon: (A) PH vs. TTP; (B) PH vs. SCD; and (C) TTP vs. SCD. Colored circles and corresponding lines of slope show different elevation classes: in green 1800–2400 m, in orange 2400–2900 m, in magenta 2900–3400 m, in black 3400–4000 m. The cyan line show the slope across all pixels without stratification by elevation class.

Table 9
R^2 values of linear fits based on 1000 randomly sampled pixels that compose the modeling dataset for Naryn rayon.

Elevation class	PH x TTP	PH x SCD	TTP x SCD
1800 – 2400 m	0.006	0.061	0.075
2400 – 2900 m	0.039	0.201	0.139
2900 – 3400 m	0.146	0.211	0.332
3400 – 4000 m	0.018	0.051	0.281
1800 – 4000 m	0.067	0.138	0.517

meaning that more negative values of the index are associated with increased precipitation. In our results, SCAND JJA was shown to have a negative relationship with PH as well, meaning more precipitation would be linked with higher PH, likely resulting from more soil moisture. However, that effect may be only evident at particular elevation belts, since in alpine and subalpine areas, precipitation may not correlate with NDVI, probably because vegetation activity is limited by low temperatures (Zhumanova et al., 2018). MEI MAM was shown in de Beurs et al. (2018) to have a positive relationship with summer precipitation. Here we found a positive relationship between MEI MAM with PH: higher MEI MAM index was linked to more summer precipitation and higher PH. Moreover, we can speculate that this increased summer precipitation could yield additional later season forage. Finally, SCAND JJA and MEI MAM were shown to be significantly negatively correlated (Table 4), which may explain why they were selected through different methods as significant influences on PH.

We also ran PLS modelling across all five rayons at two elevation classes: 2400 – 2900 m and 2900–3400 m. The results yielded that R^2 of TTP modelling dropped to ~0.27 and ~0.31 respectively (data not shown). The only significant variables, regardless of variable selection method, were snow cover metrics and slope. No seasonal oscillation index value appeared significant. In terms of PH, R^2 values were ~0.21 and ~0.27 for 2400 – 2900 m and 2900 – 3400 m, respectively (data not shown). For PH, snow cover metrics and terrain features (both slope and TRASP) were significant, but no climate oscillation index.

We posed in the introduction the question of whether the impacts of oscillation anomalies are detectable and significant in the mountain pastures using LSP metrics based on much finer spatial resolution data. Our results point to an answer of "no": at a finer spatial scale, the indirect effects of seasonal climatic oscillations are evidently overridden by terrain influences (mostly elevation) and snow cover timing. Although, while it is beyond the scope of this study, we note that changes in vegetation communities characteristics (Zhumanova et al., 2018) can result in high interannual variability in phenometrics, that in turn, may impede modeling of the linkages with oscillation modes. Moreover, the specific approach to phenometrics calculation might have introduced additional uncertainties in the analysis (Tomaszewska et al., 2019). Nevertheless, while at the fine spatial resolution of 30 m, we have not detected the indirect impacts of climate oscillations, our results do not mean that climatic teleconnections have no influence on shaping weather patterns in the region.

5. Conclusion

Although studies on much coarser scale show links between NDVI and climatic oscillation modes, and their strong influence on regional biomes (Dahlin and Ault, 2018), we did not find a significant effect at the local scale. Using much finer spatial resolution and limited spatial extent, we found overriding effects of terrain complexity, and snow cover metrics upon land surface phenology. Differences between coarser and finer spatial resolution observations increase over heterogeneous areas, and so that scale effect plays a significant role in modeling process (Liu et al., 2017; Zhang et al., 2017). Within the highland pasture land use areas of Kyrgyzstan, the heterogeneity of plant communities can be very high (Zhumanova et al., 2018) but appear homogeneous at the scale of even 30 m, which may influence land surface phenology in subtle ways. For instance, de Beurs et al. (2009) ran trend analyses of NDVI retrieved from two MODIS products at ~5.6 km and 500 m over Kazakhstan, and found that coarser scale analysis was relevant to atmospheric boundary layer processes, while the finer scale data revealed trends that were more relevant to human decision-making and regional economics. Similar cross-scale trend findings were reported using NDVI and EVI in the vegetated land surfaces of the Western Hemisphere (Heck et al., 2019).

We conclude the potential role of climatic oscillation indices informing outlooks for favorable pasture conditions in Kyrgyzstan is not feasible. One alternative approach might include focusing on those years with extreme climate oscillation values and analyze seasonal weather conditions over region to determine if those anomalies were transmitted into the phenometrics. A second alternative would be to

focus on those pixels that failed LSP modelling to investigate whether those failed fits resulted from unfavorable environmental conditions and climatic anomalies. Whether climate oscillation mode indices can provide some new and useful information about growing season conditions remains a provocative question, particularly in light of the multiple environmental challenges facing the agropastoralism livelihood in montane Central Asia.

CRediT authorship contribution statement

Monika A. Tomaszewska: Conceptualization, Data curation, Formal analysis, Software, Visualization, Writing - original draft, Writing - review & editing. **Geoffrey M. Henebry:** Conceptualization, Formal analysis, Funding acquisition, Resources, Supervision, Visualization, Writing - review & editing.

Declaration of Competing Interest

The authors declare there are no conflicts of interest associated with this research or this manuscript.

Acknowledgments

This research was supported, in part, by the NASA Land Cover / Land Use Change Program in project (NNX15AP81G) "How Environmental Change in Central Asian Highlands Impacts High Elevation Communities". We appreciate the assistance and feedback from A.A. Aidaraliev, K. Kelgenbaeva, and P. Maatkarimov. We thank the two anonymous reviewers for their helpful feedback to improve the clarity of this manuscript.

Appendix A. Supplementary data

Supplementary material related to this article can be found, in the online version, at doi:https://doi.org/10.1016/j.jag.2020.102053.

References

Abdi, H., 2003. Partial least squares (PLS) regression. In: Lewis-Beck, M., Bryman, A., Futing, T. (Eds.), Encyclopedia of Social Sciences Research Methods. SAGE Publications.

Alexander, M.A., Halimeda Kilbourne, K., Nye, J.A., 2014. Climate variability during warm and cold phases of the Atlantic Multidecadal Oscillation (AMO) 1871–2008. J. Mar. Syst. 133, 14–26. https://doi.org/10.1016/J.JMARSYS.2013.07.017.

Andersen, C.M., Bro, R., 2010. Variable selection in regression-a tutorial. J. Chemom. 24, 728–737. https://doi.org/10.1002/cem.1360.

Asian Development Bank, 2010a. Central Asia Atlas of Natural Resource. Central Asian Countries Initiative for Land Management and Asian Development Bank, Manila, Philippines.

Asian Development Bank, 2010b. Central Asian Countries Initiative for Land Management (CACILM) Multicountry Partnership Framework Support Project. [WWW Document]. https://www.adb.org/projects/38464-012/main.. .

Azykova, E.K., 2002. Geographyical and landscape characteristics of mountain territories. In: Aidaraliev, A.A. (Ed.), Mountains of Kyrgyzstan. Technology. Bishkek.

Barlow, M., Cullen, H., Lyon, B., 2002. Drought in central and Southwest Asia: La Nia, the Warm Pool, and Indian Ocean Precipitation. J. Clim. 15, 697–700. https://doi.org/10.1175/1520-0442(2002)015<0697:DICASA>2.0.CO;2.

Barnston, A.G., Livezey, R.E., 1987. Classification, seasonality and persistence of low-frequency atmospheric circulation patterns. Mon. Weather Rev. https://doi.org/10.1175/1520-0493.

Bjerksen, J., 1969. Atmospheric teleconnections from the equatorial pacific. Mon. Weather Rev. 97, 163–172. https://doi.org/10.1175/1520-0493(1969)097<0163:ATFTEP>2.3.CO;2.

Böhner, J., 2006. General climatic controls and topoclimatic variations in Central and High Asia. Boreas 35, 279–295. https://doi.org/10.1111/j.1502-3885.2006.tb01158.x.

Bohovic, R., Dobrovolny, P., Klein, D., 2016. The spatial and temporal dynamics of remotely-sensed vegetation phenology in Central Asia in the 1982–2011 period. Eur. J. Remote Sens. 49, 279–299. https://doi.org/10.5721/EuJRS20164916.

Bothe, O., Fraedrich, K., Zhu, X., 2012. Precipitation climate of Central Asia and the large-scale atmospheric circulation. Theor. Appl. Climatol. 108, 345–354. https://doi.org/10.1007/s00704-011-0537-2.

Buermann, W., Anderson, B., Tucker, C.J., Dickinson, R.E., Lucht, W., Potter, C.S., Myneni, R.B., 2003. Interannual covariability in Northern Hemisphere air temperatures and greenness associated with El Niño-Southern Oscillation and the Arctic Oscillation. J. Geophys. Res. Atmos. 108https://doi.org/10.1029/2002JD002630. n/a-n/a.

Bulut, E., Alma, Ö., 2012. A performance assessment of model selection criteria when the number of objects is much larger than the number of variables in PLSR. Eur. J. Appl. Sci. 4, 257–264. https://doi.org/10.5829/idosi.ejas.2012.4.6.1111.

Casanueva, A., Rodríguez-Puebla, C., Frías, M.D., González-Reviriego, N., 2014. Variability of extreme precipitation over Europe and its relationships with teleconnection patterns. Hydrol. Earth Syst. Sci. Discuss. 18, 709–725. https://doi.org/10.5194/hess-18-709-2014.

Chong, I., Jun, C., 2005. Performance of some variable selection methods when multicollinearity is present. Chemometr. Intell. Lab. Syst. 78, 103–112. https://doi.org/10.1016/J.CHEMOLAB.2004.12.011.

Cook, B.I., Smith, T.M., Mann, M.E., 2005. The North Atlantic Oscillation and regional phenology prediction over Europe. Glob. Chang. Biol. 11, 919–926. https://doi.org/10.1111/j.1365-2486.2005.00960.x.

CPC-NOAA, 2019. National Oceanographic and Atmospheric Administration (NOAA) Climate Prediction Center (CPC). [WWW Document]. https://www.cpc.ncep.noaa.gov/data/teledoc/telecontents.shtml.. .

Dahlin, K.M., Ault, T.R., 2018. Global linkages between teleconnection patterns and the terrestrial biosphere. Int. J. Appl. Earth Obs. Geoinf. 69, 56–63. https://doi.org/10.1016/J.JAG.2018.02.017.

de Beurs, K.M., Wright, C.K., Henebry, G.M., 2009. Dual scale trend analysis for evaluating climatic and anthropogenic effects on the vegetated land surface in Russia and Kazakhstan. Environ. Res. Lett. 4, 045012. https://doi.org/10.1088/1748-9326/4/4/045012.

de Beurs, K.M., Henebry, G.M., 2010. Spatio-Temporal Statistical Methods for Modelling Land Surface Phenology. In: Hudson, I.L., Keatley, M.R. (Eds.), Phenological Research. Springer Science+Business Media B.V., Dordrecht, pp. 177–208. https://doi.org/10.1007/978-90-481-3335-2_9.

de Beurs, K.M., Henebry, G.M., 2008. Northern annular mode effects on the land surface phenologies of northern Eurasia. J. Clim. 21, 4257–4279. https://doi.org/10.1175/2008JCLI2074.1.

de Beurs, K.M., Henebry, G.M., 2004. Land surface phenology, climatic variation, and institutional change: analyzing agricultural land cover change in Kazakhstan. Remote Sens. Environ. 89, 497–509. https://doi.org/10.1016/J.RSE.2003.11.006.

de Beurs, K.M., Henebry, G.M., Owsley, B.C., Sokolik, I.N., 2018. Large scale climate oscillation impacts on temperature, precipitation and land surface phenology in Central Asia. Environ. Res. Lett. 13, 065018. https://doi.org/10.1088/1748-9326/aac4d0.

de Beurs, K.M., Henebry, G.M., Owsley, B.C., Sokolik, I.N., 2015. Using multiple remote sensing perspectives to identify and attribute land surface dynamics in Central Asia 2001-2013. Remote Sens. Environ. 170, 48–61. https://doi.org/10.1016/j.rse.2015.08.018.

Efron, B., Tibshirani, R., 1993. An Introduction to the Bootstrap. Chapman and Hall/CRC.

ERL-NOAA, 2019. NOAA Earth Research Laboratory. [WWW Document].. .

Faber, N.M., 2002. Uncertainty estimation for multivariate regression coefficients. Chemometr. Intell. Lab. Syst. 64, 169–179. https://doi.org/10.1016/S0169-7439(02)00102-8.

Farrés, M., Platikanov, S., Tsakovski, S., Tauler, R., 2015. Comparison of the variable importance in projection (VIP) and of the selectivity ratio (SR) methods for variable selection and interpretation. J. Chemom. 29, 528–536. https://doi.org/10.1002/cem.2736.

Fieller, E.C., Hartley, H.O., Pearson, E.S., 1957. Tests for rank correlation coefficients. I. Biometrika 44, 470. https://doi.org/10.2307/2332878.

Fisher, J.I., Mustard, J.F., Vadeboncoeur, M.A., 2006. Green leaf phenology at Landsat resolution: scaling from the field to the satellite. Remote Sens. Environ. 100, 265–279. https://doi.org/10.1016/J.RSE.2005.10.022.

Geladi, P., Kowalski, B.R.R., 1986. Partial least-squares regression: a tutorial. Anal. Chim. Acta 185, 1–17.

Gerlitz, L., Steirou, E., Schneider, C., Moron, V., Vorogushyn, S., Merz, B., Gerlitz, L., Steirou, E., Schneider, C., Moron, V., Vorogushyn, S., Merz, B., 2018. Variability of the Cold Season Climate in Central Asia. Part I: Weather Types and Their Tropical and Extratropical Drivers. J. Clim. 31, 7185–7207. https://doi.org/10.1175/JCLI-D-17-0715.1.

Giorgi, F., 2006. Climate change hot-spots. Geophys. Res. Lett. 33, 1–4. https://doi.org/10.1029/2006GL025734.

Gong, D., Shi, P., 2003. Northern hemispheric NDVI variations associated with large-scale climate indices in spring. Int. J. Remote Sens. 24, 2559–2566. https://doi.org/10.1080/0143116031000075107.

Goodin, D.G., Henebry, G.M., 1997. A technique for monitoring ecological disturbance in tallgrass prairie using seasonal NDVI trajectories and a discriminant function mixture model. Remote Sens. Environ. 61, 270–278. https://doi.org/10.1016/S0034-4257(97)00043-6.

Groffman, P.M., Driscoll, C.T., Fahey, T.J., Hardy, J.P., Fitzhugh, R.D., Tierney, G.L., 2001. Colder soils in a warmer world: a snow manipulation study in a northern hardwood forest ecosystem. Biogeochemistry 56, 135–150. https://doi.org/10.1023/A:1013039830323.

Hall, D.K., Riggs, G.A., Salomonson, V.V., DiGirolamo, N.E., Bayr, K.J., 2002. MODIS snow-cover products. Remote Sens. Environ. 83, 181–194. https://doi.org/10.1016/S0034-4257(02)00095-0.

Heck, E., de Beurs, K.M., Owsley, B.C., Henebry, G.M., 2019. Evaluation of the MODIS collections 5 and 6 for change analysis of vegetation and land surface temperature dynamics in North and South America. ISPRS J. Photogramm. Remote Sens. 156, 121–134. https://doi.org/10.1016/J.ISPRSJPRS.2019.07.011.

Henebry, G.M., 2019. Methodology II: remote sensing of change in grasslands. In: Gibson,

D., Newman, J. (Eds.), Grasslands and Climate Change. Cambridge University Press, pp. 40–64. https://doi.org/10.1017/9781108163941.005.
Henebry, G.M., 2013. Phenologies of North American grasslands and grasses. In: Schwartz, M.D. (Ed.), Phenology: An Integrative Environmental Science. Springer, Netherlands, Dordrecht, pp. 197–210. https://doi.org/10.1007/978-94-007-6925-0.
Henebry, G.M., de Beurs, K.M., 2013. Remote sensing of Land surface phenology: a prospectus. Phenology: An Integrative Environmental Science. Springer, Netherlands, Dordrecht, pp. 385–411. https://doi.org/10.1007/978-94-007-6925-0_21.
Hoppe, F., Zhusui Kyzy, T., Usupbaev, A., Schickhoff, U., 2016. Rangeland degradation assessment in Kyrgyzstan: vegetation and soils as indicators of grazing pressure in Naryn Oblast. J. Mt. Sci. 13, 1567–1583. https://doi.org/10.1007/s11629-016-3915-5.
Horel, J.D., Wallace, J.M., 1981. Planetary-scale atmospheric phenomena associated with the Southern Oscillation. Mon. Weather Rev. 109, 813–829 https://doi.org/10.1175/1520-0493(1981)109<0813:PSAPAW>2.0.CO;2.
Hurrell, J.W., 1995. Decadal trends in the north atlantic oscillation: regional temperatures and precipitation. Science (80-.) 269https://doi.org/10.1126/science.269.5224.676. 676–9.
Hurrell, J.W., Kushnir, Y., Ottersen, G., 2003. An overview of the North Atlantic Oscillation. In: Hurrell, J.W., Kushnir, Y., Ottersen, G., Visbeck, M., Visbeck, M.H. (Eds.), The North Atlantic Oscillation: Climatic Significance and Environmental Impact. AGU, Washington, D.C, pp. 1–35. https://doi.org/10.1029/134GM01.
Iglesias, I., Lorenzo, M.N., Taboada, J.J., 2014. Seasonal predictability of the East Atlantic Pattern from sea surface temperatures. PLoS One 9, e86439. https://doi.org/10.1371/journal.pone.0086439.
Jiang, L., Guli, J., Bao, A., Guo, H., Ndayisaba, F., 2017. Vegetation dynamics and responses to climate change and human activities in Central Asia. Sci. Total Environ. 599–600, 967–980. https://doi.org/10.1016/J.SCITOTENV.2017.05.012.
Jolliffe, I.T., Cadima, J., 2016. Principal component analysis: a review and recent developments. Philos. Trans. R. Soc. A Math. Phys. Eng. Sci. 374, 20150202. https://doi.org/10.1098/rsta.2015.0202.
Kariyeva, J., van Leeuwen, W.J.D., 2011. Environmental drivers of NDVI-Based vegetation phenology in Central Asia. Remote Sens. (Basel) 3, 203–246. https://doi.org/10.3390/rs3020203.
Kariyeva, J., van Leeuwen, W.J.D., Woodhouse, C.A., 2012. Impacts of climate gradients on the vegetation phenology of major land use types in Central Asia (1981–2008). Front. Earth Sci. 6, 206–225. https://doi.org/10.1007/s11707-012-0315-1.
Kerr, R.A., 2000. A North Atlantic climate pacemaker for the centuries. Sci. 288, 1984–1985. https://doi.org/10.1126/science.288.5473.1984.
Kobayashi, S., Ota, Y., Harada, Y., Ebita, A., Moriya, M., Onoda, H., Onogi, K., Kamahori, H., Kobayashi, C., Endo, H., Miyaoka, K., Takahashi, K., 2015. The JRA-55 reanalysis: general specifications and basic characteristics. J. Meteorol. Soc. Japan. Ser. II 93, 5–48. https://doi.org/10.2151/jmsj.2015-001.
Krehbiel, C., Henebry, G., 2016. A comparison of multiple datasets for monitoring thermal time in urban areas over the U.S. Upper Midwest. Remote Sens. (Basel) 8, 297. https://doi.org/10.3390/rs8040297.
Krehbiel, C., Zhang, X., Henebry, G., 2017. Impacts of thermal time on land surface phenology in urban areas. Remote Sens. (Basel) 9, 499. https://doi.org/10.3390/rs9050499.
Kucheryavski, S., 2019. Mdatool.
Lehmann, E.L., D'Abrera, H.J.M., 2006. Nonparametrics: Statistical Methods Based on Ranks. Springer.
Li, J., Fan, K., Xu, Z., 2016. Links between the late wintertime North Atlantic Oscillation and springtime vegetation growth over Eurasia. Clim. Dyn. 46, 987–1000. https://doi.org/10.1007/s00382-015-2627-9.
Li, S., Perlwitz, J., Quan, X., Hoerling, M.P., 2008. Modelling the influence of North Atlantic multidecadal warmth on the Indian summer rainfall. Geophys. Res. Lett. 35, L05804. https://doi.org/10.1029/2007GL032901.
Liu, Y., Hill, M.J., Zhang, X., Wang, Z., Richardson, A.D., Hufkens, K., Filippa, G., Baldocchi, D.D., Ma, S., Verfaillie, J., Schaaf, C.B., 2017. Using data from Landsat, MODIS, VIIRS and PhenoCams to monitor the phenology of California oak/grass savanna and open grassland across spatial scales. Agric. For. Meteorol 237–238, 311–325. https://doi.org/10.1016/J.AGRFORMET.2017.02.026.
Liu, Y., Wang, L., Zhou, W., Chen, W., 2014. Three Eurasian teleconnection patterns: spatial structures, temporal variability, and associated winter climate anomalies. Clim. Dyn. 42, 2817–2839. https://doi.org/10.1007/s00382-014-2163-z.
Lu, L., Guo, H., Kuenzer, C., Klein, I., Zhang, L., Li, X., 2014. Analyzing phenological changes with remote sensing data in Central Asia. IOP Conf. Ser. Earth Environ. Sci. 17, 012005. https://doi.org/10.1088/1755-1315/17/1/012005.
Mehmood, T., Liland, K.H., Snipen, L., Sæbø, S., 2012. A review of variable selection methods in Partial Least Squares Regression. Chemometr. Intell. Lab. Syst. 118, 62–69. https://doi.org/10.1016/J.CHEMOLAB.2012.07.010.
Melaas, E.K., Friedl, M.A., Zhu, Z., 2013. Detecting interannual variation in deciduous broadleaf forest phenology using Landsat TM/ETM + data. Remote Sens. Environ. 132, 176–185. https://doi.org/10.1016/J.RSE.2013.01.011.
Menzel, A., Sparks, T.H., Estrella, N., Eckhardt, S., 2005. "SSW to NNE" - North Atlantic Oscillation affects the progress of seasons across Europe. Glob. Chang. Biol. 11, 909–918. https://doi.org/10.1111/j.1365-2486.2005.00954.x.
Myneni, R.B., Hall, F.G., Sellers, P.J., Marshak, A.L., 1995. The interpretation of spectral vegetation indexes. IEEE Trans. Geosci. Remote Sens. 33, 481–486. https://doi.org/10.1109/TGRS.1995.8746029.
NASA, J.P.L., 2013. NASA Shuttle Radar Topography Mission Global 1 Arc Second. [Data set] [WWW Document]. NASA EOSDIS L. Process. DAAC.. https://doi.org/10.5067/MEaSUREs/SRTM/SRTMGL1.003.
National Weather Service, 2019. Climate Prediction Center, Teleconnection Index Calculation Procedures. [WWW Document]. https://www.cpc.ncep.noaa.gov/data/teledoc/teleindcalc.shtml.. .
Nguyen, L.H., Joshi, D.R., Clay, D.E., Henebry, G.M., 2018. Characterizing land cover/land use from multiple years of Landsat and MODIS time series: a novel approach using land surface phenology modeling and random forest classifier. Remote Sens. Environ. https://doi.org/10.1016/J.RSE.2018.12.016.
Peel, M.C., Finlayson, B.L., McMahon, T.A., 2007. Updated world map of the Köppen-Geiger climate classification. Hydrol. Earth Syst. Sci. Discuss. 11, 1633–1644. https://doi.org/10.5194/hess-11-1633-2007.
Qiao, D., Wang, N., 2019. Relationship between Winter Snow Cover Dynamics, Climate and Spring Grassland Vegetation Phenology in Inner Mongolia, China. ISPRS Int. J. Geo-Information 8, 42. https://doi.org/10.3390/ijgi8010042.
Rajalahti, T., Arneberg, R., Berven, F.S., Myhr, K., Ulvik, R.J., Kvalheim, O.M., 2009a. Biomarker discovery in mass spectral profiles by means of selectivity ratio plot. Chemometr. Intell. Lab. Syst. 95, 35–48. https://doi.org/10.1016/J.CHEMOLAB.2008.08.004.
Rajalahti, T., Arneberg, R., Kroksveen, A., Berle, M., Myhr, K., Kvalheim, O., 2009b. Discriminating variable test and selectivity ratio plot: quantitative tools for interpretation and variable (Biomarker) selection in complex spectral or chromatographic profiles. Anal. Chem. 81, 2581–2590. https://doi.org/10.1021/ac802514y.
Riggs, G.A., Hall, D.K., 2015. MODIS Snow Products Collection 6 User Guide.
Riggs, G.A., Hall, D.K., 2004. Snow mapping with the MODIS Aqua instrument. 61st East. Snow Conf.
Roberts, D.W., Cooper, S.V., 1989. Concepts and Techniques of Vegetation Mapping. In Land Classifications Based on Vegetation. Applications for Resource Management, Ogden, UT.
Rodwell, M.J., Rowell, D.P., Folland, C.K., 1999. Oceanic forcing of the wintertime North Atlantic Oscillation and European climate. Nature 398, 320–323. https://doi.org/10.1038/18648.
Roy, D.P., Kovalskyy, V., Zhang, H.K., Vermote, E.F., Yan, L., Kumar, S.S., Egorov, A., 2016. Characterization of Landsat-7 to Landsat-8 reflective wavelength and normalized difference vegetation index continuity. Remote Sens. Environ. 185, 57–70. https://doi.org/10.1016/J.RSE.2015.12.024.
Schillhorn Van Veen, T.W., 1995. The Kyrgyz Sheep Herders at a Crossroads. Overseas Dev. Institute. Pastor. Dev. Netw. Ser.
Still, C.J., Pau, S., Edwards, E.J., 2014. Land surface skin temperature captures thermal environments of C_3 and C_4 grasses. Glob. Ecol. Biogeogr. 3, 286–296. https://doi.org/10.1111/geb.12121.
Syed, F.S., Giorgi, F., Pal, J.S., King, M.P., 2006. Effect of remote forcings on the winter precipitation of central southwest Asia part 1: observations. Theor. Appl. Climatol. 86, 147–160. https://doi.org/10.1007/s00704-005-0217-1.
Tenenhaus, M., 1998. La Regression PLS. Technip, Paris.
Tomaszewska, M.A., Henebry, G.M., 2018. Changing snow seasonality in the highlands of Kyrgyzstan. Environ. Res. Lett. 13, 065006. https://doi.org/10.1088/1748-9326/aabd6f(1).
Tomaszewska, M.A., Nguyen, L.N., Henebry, G.M., 2019. Land surface phenology in the highland pastures of montane central asia: interactions with snow cover seasonality and terrain characteristics. Remote Sens. Environ In review.
Tran, T.N., Afanador, N.L., Buydens, L.M.C., Blanchet, L., 2014. Interpretation of variable importance in partial least squares with significance multivariate correlation (sMC). Chemometr. Intell. Lab. Syst. 138, 153–160. https://doi.org/10.1016/J.CHEMOLAB.2014.08.005.
Tucker, C.J., 1979. Red and photographic infrared linear combinations for monitoring vegetation. Remote Sens. Environ. 8, 127–150. https://doi.org/10.1016/0034-4257(79)90013-0.
USGS EROS, 2017. Landsat Collection 1 Level 1 Product Definition. Sioux Falls, SD.
Vetter, S., 2005. Rangelands at equilibrium and non-equilibrium: recent developments in the debate. J. Arid Environ. 62, 321–341. https://doi.org/10.1016/J.JARIDENV.2004.11.015.
Viña, A., Henebry, G.M., 2005. Spatio-temporal change analysis to identify anomalous variation in the vegetated land surface: ENSO effects in tropical South America. Geophys. Res. Lett. 32, 1–5. https://doi.org/10.1029/2005GL023407.
Wan, Z., Hook, S., Hulley, G., 2015. MOD11A2 MODIS/Terra Land Surface Temperature/Emissivity 8-Day L3 Global 1km SIN Grid V006.
Wang, C., Xie, S., Carton, J.A., 2004. A global survey of ocean-atmosphere interaction and climate variability. In: Wang, C., Xie, S., Carton, J. (Eds.), Earth's Climate: The Ocean-Athmosphere Interaction. AGU, Washington, DC, pp. 1–19. https://doi.org/10.1029/147GM01.
Wang, G., Schimel, D., 2003. Climate change, climate modes, and climate impacts. Annu. Rev. Environ. Resour. 28, 1–28. https://doi.org/10.1146/annurev.energy.28.050302.105444.
Wold, H.O.A., 1982. Soft modeling: the basic design and some extensions. In: Jöreskog, K.G., Wold, H.O.A. (Eds.), Systems Under Indirect Observations: Part II. North-Holland, Amsterdam, pp. 1–54.
Wold, H.O.A., 1966. Estimation of principal components and related models by iterative least squares. In: Krishnajah, P.R. (Ed.), Multivariate Analysis. Academic Press., New York, NY, pp. 391–420.
Wold, S., 1987. Principal component analysis. Chemometr. Intell. Lab. Syst. 2, 37–52.
Wold, S., Johansson, E., Cocchi, M., 1993. PLS: partial least squares projections to latent structures. In: Kubinyi, H. (Ed.), 3D QSAR in Drug Design. Volume 1: Theory Methods and Applications. Springer, Netherlands, pp. 523–550.
Wold, S., Ruhe, A., Wold, H., Dunn III., W.J., 1984. The collinearity problem in linear regression. The partial least squares (PLS) approach to generalized inverses. SIAM J. Sci. Stat. Comput. 5, 735–743. https://doi.org/10.1137/0905052.
Wold, S., Sjöström, M., Eriksson, L., 2001. PLS-regression: a basic tool of chemometrics. Chemometr. Intell. Lab. Syst. 58, 109–130. https://doi.org/10.1016/S0169-7439(01)00155-1.

Wolter, K., Timlin, M.S., 2011. El Niño/Southern Oscillation behaviour since 1871 as diagnosed in an extended multivariate ENSO index (MEI.ext). Int. J. Climatol. 31, 1074–1087. https://doi.org/10.1002/joc.2336.

Wolter, K., Timlin, M.S., 1993. Monitoring ENSO in COADS with a seasonally adjusted principal component index. In: Proceedings of the 17th Climate Diagnostics Workshop. Norman, OK. pp. 52–57.

Wright, C.K., de Beurs, K.M., Henebry, G.M., 2014. Land surface anomalies preceding the 2010 Russian heat wave and a link to the North Atlantic Oscillation. Environ. Res. Lett. 9, 124015. https://doi.org/10.1088/1748-9326/9/12/124015.

Yeh, S., Cai, W., Min, S., McPhaden, M., Dommenget, D., Dewitte, B., Collins, M., Ashok, K., An, S., Yim, B., Kug, J., 2018. ENSO atmospheric teleconnections and their response to greenhouse gas forcing. Rev. Geophys. 56, 185–206. https://doi.org/10.1002/2017RG000568.

Yin, Z., Wang, H., Liu, X., 2014. A comparative study on precipitation climatology and interannual variability in the lower midlatitude East Asia and Central Asia. J. Clim. 27, 7830–7848. https://doi.org/10.1175/JCLI-D-14-00052.1.

Zhang, X., Wang, J., Gao, F., Liu, Y., Schaaf, C., Friedl, M., Yu, Y., Jayavelu, S., Gray, J., Liu, L., Yan, D., Henebry, G.M., 2017. Exploration of scaling effects on coarse resolution land surface phenology. Remote Sens. Environ. 190, 318–330. https://doi.org/10.1016/J.RSE.2017.01.001.

Zhumanova, M., Mönnig, C., Hergarten, C., Darr, D., Wrage-Mönnig, N., 2018. Assessment of vegetation degradation in mountainous pastures of the Western Tien-Shan, Kyrgyzstan, using eMODIS NDVI. Ecol. Indic. 95, 527–543. https://doi.org/10.1016/j.ecolind.2018.07.060.

Zhumanova, M., Wrage-Mönnig, N., Darr, D., 2016. Farmers' decision-making and land use changes in Kyrgyz agropastoral systems. Res. Dev. 36, 506–517. https://doi.org/10.1659/MRD-JOURNAL-D-16-00030.1.